ABSTRACT

STUDY OF THE SYSTEMATIC UNCERTAINTIES ASSOCIATED WITH THE TRACKING DETECTORS

Daniel W. Boyden, MS.
Department of Physics
Northern Illinois University, 2019
Michael Eads, Director

The muon g-2 experiment at Fermilab looks to measure the anomalous magnetic moment of the muon to an unprecedented precision of 0.14 ppm to verify results from the E821 experiment at Brookhaven National Laboratory. In addition to the anomalous magnetic moment of the muon the project also seeks to measure the muon electric dipole moment to a better precision than has previously has been achieved. These measurement along with standard model predictions may result in a discrepancy between the standard model and experimental results which may give some insight to beyond standard model physics.

This thesis I will present the results for systematics studies from the straw tube trackers in this experiment; mainly the resolution and cross talk in the detectors. I will also present how this will vary with a few of the final measurements for this experiment.

NORTHERN ILLINOIS UNIVERSITY
DE KALB, ILLINOIS

JULY 2019

STUDY OF THE SYSTEMATIC UNCERTAINTIES ASSOCIATED WITH THE TRACKING DETECTORS

BY

DANIEL W. BOYDEN

A THESIS SUBMITTED TO THE GRADUATE SCHOOL

IN PARTIAL FULFILLMENT OF THE REQUIREMENTS

FOR THE DEGREE

MASTERS OF SCIENCE

DEPARTMENT OF PHYSICS

Thesis Director:
Michael Eads

ACKNOWLEDGEMENTS

I would like to thank my advisor Micheal Eads for his financial support, and guidance in completing this research. He has been extremely patient and kind with me while completing the research for this thesis which allowed me to gather a great deal of knowledge that I otherwise would have never been able to do elsewhere.

I would like to thank my committee members, Mike Syphers, and David Hedin. During our meeting they have given me there valuable insight which helped give me direction for my research.

I would also like to thank all of the professors in the department for giving me the opportunity to study at NIU and giving me direction throughout the course of graduate school.

TABLE OF CONTENTS

LIST OF TABLES

Table Page

LIST OF FIGURES

Figure Page

Figure Page

LIST OF TABLES

LIST OF FIGURES

CHAPTER 1

INTRODUCTION TO THE MUON G-2 EXPERIMENT

In the following chapter there will be an explanation of the history of the experiment, why the experiment is being performed, along with the fundamental aspects of GM2. Furthermore, there will be an explanation of the results from the previous experiment E821 and how this relates to standard model predictions. This gives the fundamental reasoning for performing E989, the current G-2 experiment.

1.1 History and Motivation

The muon anomalous magnetic moment has been measured in a series of experiments at CERN and more recently in the E821 experiment at the Brookhaven National Laboratory. In the first CERN measurements, muons were injected into a 6-m long straight magnet where they followed a drifting spiral path slowly traversing the magnet because of a small gradient introduced in the field. The muons were topped in a polarimeter outside the magnet and the measurement of their net spin precession determined with an uncertainty of 4300 ppm. The results agreed with the prediction of QED for a structureless particle.[1] The second CERN experiment used a magnetic ring to extend the muon storage time. The muon precession frequency was measured by the number of decayed positrons versus time and observing the precession frequency of the decayed positrons. They were able to determine the value of to an uncertainty of 270 ppm, which agreed with theory only after the three-photon exchange contribution to the sixth-order anomalous magnetic moment were included.[2] Furthermore,

the third CERN experiment also used a magnetic storage ring with a much higher rate and was able to determine the value to within an uncertainty of 10 ppm, which also agreed with theory.[3] The most recent Brookhaven Experiment, E821, followed the same principles as the third CERN experiment but having multiple improvements in the field uniformity and increased storage efficiency. E821 was able to determine to an uncertainty of 0.54 ppm. Ref.[4]

1.1.1 Magnetic and Electric Dipole Moments

The study of magnetic moments started with the development of quantum mechanics. For fermions it is related to the spin by the Eq.1.6. This is derived from the fact that if there is circular loop of a wire carrying a current I with a cross sectional area A, it produces a magnetic moment μ. The current is given by Eq.1.2 where q is the charge, r is the radius of the loop, and $Q = \pm 1$ taking account of the charge. The area is given by Eq.1.3 where v would be the velocity of the particle.

$$\vec{\mu} = I\vec{A} \tag{1.1}$$

$$I = \frac{Qqv}{2\pi r} \tag{1.2}$$

$$A = \pi r^2 \tag{1.3}$$

By plugging in Eq.1.2 and Eq.1.3 into Eq.1.1 yields Eq.1.4.

$$\vec{\mu} = \frac{Qq}{2m}\vec{L} \tag{1.4}$$

Using the relation of angular momentum $L = mvr$ and knowing the only contribution to angular momentum of a free particle is due only to its spin this gives Eq.1.5. In the modern interpretation of the Stern Gerlach experiment which observed that the spin is quantized and 1.5 is off by a factor of 2.[5] To correct for this there was added a fudge factor called the g-factor giving 1.6. Although, coming to this conclusion required the discovery of the spin, quantum mechanics, and Thomas' relativistic correction. Where Thomas' correction applies to the spin of an elementary particle and relates the angular velocity of the spin to the angular velocity of the particles motion.

$$\vec{\mu} = \frac{Qq}{2m}\vec{s} \tag{1.5}$$

$$\vec{\mu} = g\frac{Qq}{2m}\vec{s} \tag{1.6}$$

In 1928 Dirac applied special relativity to Schrodinger's equation. Dirac's relativistic theory predicted that $g = 2$. In 1933 Stern showed that that the g-factor of the proton was approximately 5.5 which proved that the proton was not a pure Dirac particle.[8] In addition, Alvarez and Bloch discovered the neutron had a large magnetic moment which was not expected.[6] In 1947, motivated by measurements of the hyperfine structure in hydrogen, Schwinger showed that from a theoretical standpoint this splitting can be accounted for by adding in a term for the electron spin magnetic moment for the lowest radiative correction to the Dirac moment.[7]

$$\frac{\delta\mu}{\mu} = \frac{1}{2\pi}\frac{e^2}{\hbar c} \tag{1.7}$$

It has been found useful to break the magnetic dipole moment into two terms as follows with a being the anomalous magnetic moment. Ref.[4]

$$\mu = (1 + a)\frac{e\hbar}{2m} \tag{1.8}$$

Where

$$a = \frac{g - 2}{2} \tag{1.9}$$

1.1.2 The Muon

The muon was first observed in a Wilson cloud chamber by Kunze in 1933.[9] In 1936, Anderson and Neddermeyer reported that the muon is less massive than the proton but more penetrating than the electron.[10] Muon decays through the force $\mu^- \rightarrow e^- \nu_\mu \overline{\nu}_e$. With the muons long lifetime of approximately 2.2 μs this permits precession measurements of its mass, lifetime, and magnetic moment which makes the muon a good candidate for experiments.[4]

1.1.3 The Muon Magnetic Moment

The muon magnetic moment played an important role in the discover of the generation structure of the standard model. The muon spin experiment at Nevis Cyclotron witnessed parity violation in muon decays, in addition to showing that g_μ is consistent with 2. Later experiments showed that in a magnetic field the muon behaves like a heavy electron. Ref.[4]

1.1.4 The Muon Electric Dipole Moment

In his relativistic theory Dirac discovered an EDM and like the magnetic dipole moment, the EDM must be in the direction of the spin. The equation for the Electric dipole moment is given by Eq.1.10.

$$\vec{d} = \eta(\frac{Qe}{2mc})\vec{s} \tag{1.10}$$

Where η is dimensionless and analogous to g in Eq. 1.6. An EDM is forbidden by parity and by time reversal which was first pointed out by Landau and Ramsey by examining the Hamiltonian given by Eq.1.11. [11]

$$H = -\vec{\mu} \cdot \vec{B} - \vec{d} \cdot \vec{E} \tag{1.11}$$

Therefore, searches for a permanent EDM of electrons, neutrons, and atomic nucleus have become an important search for physics beyond the standard model. Ref.[4]

1.2 Quick Summary of Experimental Technique

In the modern G-2 experiment E989, a polarized beam of muons is produced and injected into a storage ring from the Fermilab accelerator complex. The magnetic field is a dipole field in the storage ring with vertical focusing being provided by the electrostatic quadrupoles. There are two frequencies are measured experimentally, the first frequency ω_a is the rate at which the muon polarization turns relative to the momentum of the muon, and the second frequency ω_p is the value of the magnetic field normalized to the Lamour frequency.

$$\vec{\omega}_a = \vec{\omega}_S - \vec{\omega}_C \tag{1.12}$$

Where S denotes the spin and C denotes the cyclotron which the individual terms are given by Eq.1.13 and Eq.1.14

$$\omega_S = -g\frac{Qe}{2m}B - (1-\gamma)\frac{Qe}{\gamma m}B \tag{1.13}$$

$$\omega_C = -\frac{Qe}{m\gamma}B \tag{1.14}$$

It is worth noting that ω_a depends only on the anomaly a_μ and depends linearly on the applied magnetic field. In the presence of an electric field we get 1.27

$$\vec{\omega}_a = -\frac{Qe}{m}[a_\mu \vec{B} + (a_\mu - (\frac{m}{p})^2)\frac{\vec{\beta}\times\vec{E}}{c}] \tag{1.15}$$

If $p_{magic} = \frac{m}{\sqrt{a_\mu}} \equiv 3.09\frac{GeV}{c}$ the electric field contribution in Eq. 1.27 cancels to the first order which only requires higher order corrections to the term. The factor a_μ from the two frequencies we use the relation 1.16.

$$a_\mu = \frac{\omega_a/\omega_p}{\lambda_+ - \omega_a/\omega_p} \tag{1.16}$$

The necessary steps in the experiment consist of the following. Ref. **??**

1. Production of an appropriate pulsed proton beam from accelerator complex.
2. Production of pions using this proton beam.
3. Collection of the polarized muons from pion decay.
4. Injection of the muon beam into the storage ring.
5. Kicking the muon beam onto stored orbits

6. Measuring the arrival time and energy of positrons form the muon decays.

1.2.1 Quick Introduction to Muon Beam Dynamics

Here is given a quick introduction to the physics of the beam dynamics of a weakly focused betatron which is used in the current E989 experiment. This section is mainly used to give an introduction to the pitch correction and the radial field correction which will be discussed later in the systematics study.

Beam dynamics of the storage ring directly affects the measurement of a_μ since the detector acceptance for the decay electrons depends on the radial coordinate of the muon at the point where it decays. Resonances in the storage ring also can cause particle losses which affect the measurement. Care is taken in the experiment in setting the frequency of the coherent betatron oscillation which lies close to the second harmonic $f_a = \omega_a/2\pi$. If f_{cbo} is too close to $2 \times f_a$, which is the beat frequency, this complicates the extraction of f_a from the data and can introduce significant systematic uncertainty.

A pure quadrupole electric field supplies a linear restoring force in the vertical direction and the combination of the electric field. The central magnetic field provides a linear restoring force in the radial direction. The G-2 storage ring is a weak focusing ring with the field index given by Eq.1.17.

$$n = \frac{\kappa R_0}{\beta B_0} \tag{1.17}$$

Where κ is the electric quadrupole gradient, B_0 is the magnetic field strength, R_0 is the magic radius, and β is the relativistic velocity of the muon beam. For a ring with a uniform

vertical dipole magnetic field and a uniform quadrupole field the horizontal and vertical motion is given by Eq.1.18 and Eq.1.19 respectively.

$$x = x_e + A_x cos(\nu_x \frac{s}{R_0} + \delta_x) \tag{1.18}$$

$$y = A_y cos(\nu_y \frac{s}{R_0} + \delta_y) \tag{1.19}$$

Where s is the arc length along the trajectory of the ring. The horizontal and vertical tunes are given by Eq.1.20 and Eq.1.21 respectively.

$$\nu_x = \sqrt{1-n} \tag{1.20}$$

$$\nu_y = \sqrt{n} \tag{1.21}$$

In E821 there were several tunes used for in the data acquisition $n = 0.137, 0.142, 0.122$. The horizontal and vertical betatron frequencies are given by Eq.1.22 and Eq.1.23 repectively.

$$f_x = f_c\sqrt{1-n} \equiv 0.929 f_c \tag{1.22}$$

$$f_y = f_c\sqrt{n} \equiv 0.37 f_c \tag{1.23}$$

Where f_c is the cyclotron frequency and $n = 0.137$. The field index also determines the angular acceptance of the ring where the maximum horizontal and vertical angle of the muon momentum are given by Eq.1.24 and Eq.1.25 respectively.

$$\theta^x_{max} = \frac{x_{max}\sqrt{1-n}}{R_0} \tag{1.24}$$

$$\theta^{y}_{max} = \frac{y_{max}\sqrt{n}}{R_0} \tag{1.25}$$

Where $x_{max}, y_{max} = 45mm$ which is the radius of the storage ring aperture.

For a ring with discrete quads the focusing strength changes as a function of azimuth and the equation of motion looks like an oscillator where the spring constant constantly changes as a function of azimuth s.

$$X(s) = x_e + A\sqrt{\beta(s)}cos(\phi(s) + \delta) \tag{1.26}$$

The presence of the coherent betatron oscillation was first discovered in the E821 experiment from a plot that showed there was in azimuthal variation in a_μ so this led to a correction factor.

In the simplest case with the absence of an electric field and when the velocity is perpendicular to the magnetic field, the rate at which the spin precesses relative to the momentum is given by Eq.1.27.

$$\omega_a = -a\frac{Qe}{m}B \tag{1.27}$$

However, in the real experiment not all the muons are at the magic momentum, therefore a precision knowledge of the trajectories required. To look at this effect we calculate the effect on the electric field due to muon not directly at γ_{magic}, for the moment neglecting the $\vec{\beta} \cdot \vec{B}$ terms.

$$\omega'_a = \omega_a[1 - \beta\frac{E_r}{B_y}(1 - \frac{1}{a_\mu\beta^2\gamma^2})] \tag{1.28}$$

Where $\omega_a = -a\frac{Qe}{m}B$. Now using the fact that $p = \beta\gamma m = p_m + \Delta p$ we get Eq.1.29.

$$\frac{\Delta\omega_a}{\omega_a} = -2\frac{\beta E_r}{B_y}(\frac{\Delta P}{P_m}) \tag{1.29}$$

Where the fractional change in momentum in Eq.1.29 can be represented as Eq.1.30

$$\frac{\Delta P}{P_m} = (1-n)\frac{\Delta R}{R_0} = (1-n)\frac{X_e}{R_0} \tag{1.30}$$

Where the X_e is the muons beam equilibrium radius. Then the electric quadrupole field is given by Eq.1.31

$$E = \kappa X = \frac{n\beta B_y}{R_0}x \tag{1.31}$$

Therefore we obtain the final result to the change in frequency Eq.1.32.

$$\frac{\Delta\omega}{\omega} = -2n(1-n)\beta^2\frac{xx_e}{R_0^2 B_y} \tag{1.32}$$

Therefore, the effect of muons not at the magic momentum is to lower the measured ω_a frequency. For a quadrupole focusing field plus a uniform magnetic field the time average of $< x >= x_e$, so the electric field correction is given by Eq.1.33. The value $< x_e^2 >$ is determined in the fast rotation analysis which will not be covered in this thesis. In the Brookhaven experiment it was found for a low n that $C_E = 0.47 \pm 0.054 ppm$.

$$C_E = \frac{\Delta\omega}{\omega} = -2n(1-n)\beta^2\frac{< x_e^2 >}{R_0^2 B_y} \tag{1.33}$$

The betatron oscillations of the muon beam lead to the terms $\vec{\beta}\cdot\vec{B} \neq 0$. Since the $\vec{\beta}\cdot\vec{B}$ term is quadratic in the component of $\vec{\beta}$, its contribution to $\vec{\omega_s}$ will not generally average out to zero. The spin precession frequency has a small dependence on the betatron motion of the beam. In addition, it turns out the only significant correction comes from the vertical

betatron oscillations which is called the pitch correction. The pitch angle varies harmonically as in Eq.1.34

$$\psi = \psi_0 Cos(\omega_y t) \tag{1.34}$$

Where ω_y is the vertical betatron frequency. If we set $a_\mu - \frac{1}{\gamma^2-1} = 0$ we obtain 1.35

$$\vec{\omega}_{diff} = -\frac{Qe}{m}[a_\mu \vec{B} - a_\mu(\frac{\gamma}{\gamma+1})(\vec{\beta}\cdot\vec{B})\vec{\beta}] \tag{1.35}$$

Now if we assume that the pitch angles are small, $\vec{B} = \hat{y}B_y$, $\beta = \hat{z}\beta_z + \hat{y}\beta_y$ then the difference in frequency is given by Eq.1.36.

$$\omega'_{ay} = -\omega_a[1 - (\frac{\gamma-1}{\gamma})\psi^2] \tag{1.36}$$

This then gives the pitch correction found in Eq.1.37.

$$C_p = -\frac{<\psi^2>}{2} = -\frac{n}{4}\frac{<y^2>}{R_0^2} \tag{1.37}$$

The result that the pitch correction and the radial field corrections are dependent on the average positions is what makes straw trackers important in E989 since these detectors have the best resolution for position measurements.

1.3 Results from Brookhaven Experiment

The Brookhaven based experiment E821 which was completed in 2001 was a successful experiment in its achievements. As previously mentioned, the experiment was able to measure the precession frequency to approximately 14 times better than what was ever achieved

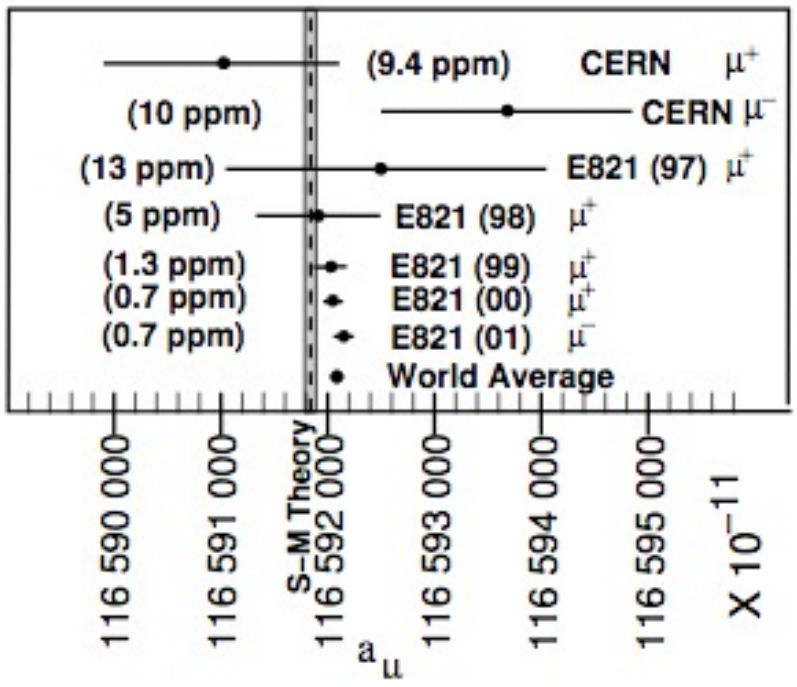

Figure 1.1: Measurement of a_μ from CERN and BNL E821. The vertical band in the SM value using the hadronic contribution. [4]

before in the previous CERN experiments. Steady improvements in the theory resulted in a present measurement of a_μ with an uncertainty of 0.42 ppm. The E821 experiment was able to reach a field uniformity to ± 1 ppm uniformity on average. The main systematical uncertainties of this experiment were caused from anything that caused the extracted frequency to vary the true fit value. Uncertainties in the ω_a measurement mainly consist of gain instability in the detectors, lost muons, spin tracking, coherent betatron oscillations, differential decays, and pitch correction uncertainties. The main source of uncertainty from the ω_p measurement consist of errors due to non-uniformity in the magnetic field. The results for E821 are given in Fig. 1.1 which show previous measurements and the Standard Model Predictions which shows that there was a discrepancy from standard model values for a_μ and the Brookhaven National Laboratory experiment measured values up to 3.5 standard deviations. Ref.[4]

CHAPTER 2

E989 EXPERIMENT AT FERMILAB

This Chapter will explain the experimental apparatus used for the E989 experiment at Fermilab. It will also cover the improvements from the previous E821 experiment at BrookHaven National laboratory and the current status of this experiment.

2.1 Explanation of Experimental Apparatus

The GM2 experiment is a complicated project with many different subsystems to improve the results from previous experiments.[4] The experiment is re-using the storage magnet and the superconducting inflector that was used in E821, with a refurbished NMR trolley and magnetic field measurement system. Mainly, the new features to E989 are that a pure muon beam has been designed and commissioned minimizing hadronic components, segmented calorimeters consisting of a 6×9 array of lead fluoride crystals to minimize ionizing particle such as lost muons, a new fast muon kicker, improved magnetic shimming to improve field variations by a factor of two, two straw tracker arrays located in the vacuum and behind the calorimeters, and a more rapid rate of data taking provided by Fermi Lab accelerator facility. The goal is to generate 21 times more data than Brookhaven and to improve the systematic errors by a factor of three and the overall uncertainty of the measurement. [4]

To produce muons in the experiment an 8 GeV pulsed proton beam coming from the recycler ring at Fermi Lab is collided with a target, producing pions. The pions are the selected by their energy and the beam is then transported into the delivery ring. During

Figure 2.1: Illustration of the Muon Campus at Fermi Lab Ref. [13]

this transportation the pions then decay into a polarized muon beam. These muons are then transported to the storage ring in the experimental hall on the muon campus. Refer to Fig.2.1 for a visual representation. [12]

The muon are injected through the inflector magnet which provides a region free of magnetic fields for the muon to pass through and into the storage ring at the MC1 building housing the storage ring. The muons are then centered in the ring using a kicker. The kicker is a series of three long plate that are able to produce a pulsed magnetic field. The magnetic field in the ring is produced by super conducting coils surrounded by iron yokes as to maintain uniformity of the magnetic field. Refer to Fig. 2.2 for a cross section schematic of the ring. As the polarized muons pass through this magnetic field they precess according to the ω_a frequency as covered in previous sections. The muon then decays into a positron preferentially in the direction of it's spin and is detected by the calorimeters and the tracker

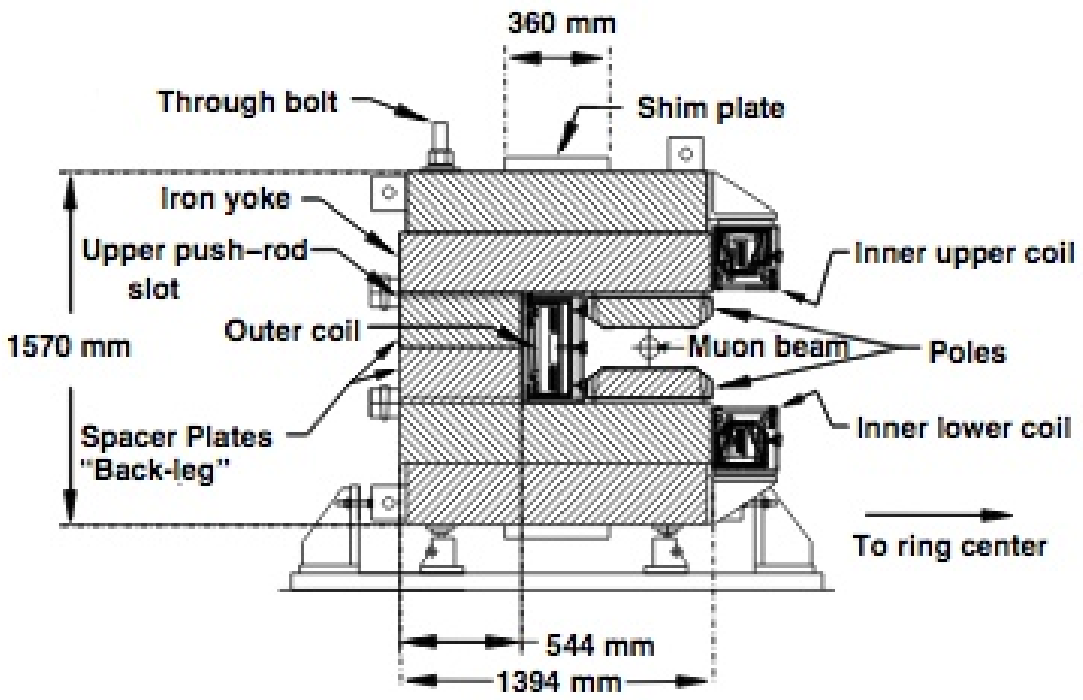

Figure 2.2: Illustration of the cross section of the storage ring Ref. [4]

stations on the inside of the ring. Shown in Fig. 2.3 is a birds eye view representation of the storage ring and the position of the kickers, inflector, tracker stations, and calorimeter stations. The detectors consist of 24 calorimeters and two tracker stations that each consist of 8 trackers.

Since uncertainties are extremely important in this experiment measurement and evaluation of the uniformity of the magnetic field is necessary. One system used for this are fixed NMR probes at several locations around the ring. A trolley system was developed that can travel throughout the ring and measure the magnetic field.

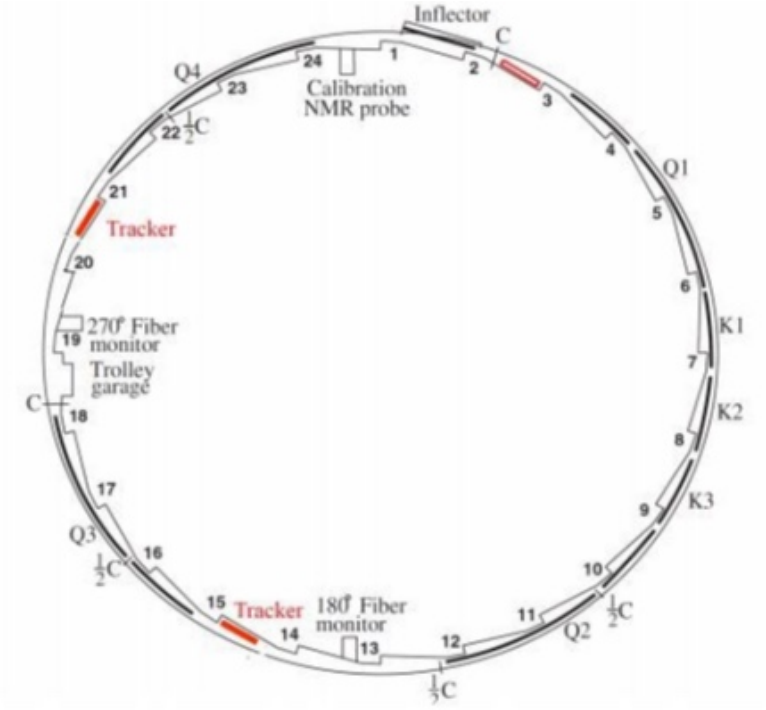

Figure 2.3: Birds Eye View of the Ring Ref. [4]

2.2 Requirements of the E989 Experiment

To meet the goal of an experimental precision of 140 ppb, 21 times more data needs to be collected than the E821 experiment. This will result in a 100 ppb statistical uncertainty in the a_μ measurement. The measurement of ω_a and ω_p have a total proposed uncertainty of 70 ppb. The proposed limits for the expected uncertainty of the experiment can be found in Fig. 2.4 and Fig.2.5.

Category	E821 [ppb]	E989 Improvement Plans	Goal [ppb]
Gain changes	120	Better laser calibration	
		low-energy threshold	20
Pileup	80	Low-energy samples recorded	
		calorimeter segmentation	40
Lost muons	90	Better collimation in ring	20
CBO	70	Higher n value (frequency)	
		Better match of beamline to ring	< 30
E and pitch	50	Improved tracker	
		Precise storage ring simulations	30
Total	180	Quadrature sum	70

Figure 2.4: Expected Improvement in the systematic uncertainties for ω_a . Ref [4]

Category	E821 [ppb]	Main E989 Improvement Plans	Goal [ppb]
Absolute field calibration	50	Special 1.45 T calibration magnet with thermal enclosure; additional probes; better electronics	35
Trolley probe calibrations	90	Plunging probes that can cross calibrate off-central probes; better position accuracy by physical stops and/or optical survey; more frequent calibrations	30
Trolley measurements of B_0	50	Reduced position uncertainty by factor of 2; improved rail irregularities; stabilized magnet field during measurements*	30
Fixed probe interpolation	70	Better temperature stability of the magnet; more frequent trolley runs	30
Muon distribution	30	Additional probes at larger radii; improved field uniformity; improved muon tracking	10
Time-dependent external magnetic fields	–	Direct measurement of external fields; simulations of impact; active feedback	5
Others †	100	Improved trolley power supply; trolley probes extended to larger radii; reduced temperature effects on trolley; measure kicker field transients	30
Total systematic error on ω_p	170		70

Figure 2.5: Expected Improvement in the systematic uncertainties for ω_p. Ref. [4]

CHAPTER 3

STRAW TUBE TRACKING IN E989

This chapter provides a brief introduction to the straw tube tracking fundamentals, the design of the trackers, and the terminology that will be used in later sections. Furthermore, an explanation of the tracking algorithms and how the software used is composed so that there is a further understanding of the motivation and how specifically the goals of the study have been achieved.

3.1 Straw Tube Trackers

The straw tube trackers in E989 are a fundamental aspect in the measurement. In addition, the straws are an important part in measuring the beam profile in the experiment and can serve as a double check of the calorimeters. These measurement can be done purely by using the calorimeters in the experiment, however the spatial resolution of the straw trackers will greatly reduce the uncertainty in the measurement.

3.1.1 Basic Design of the Straw Tube Trackers

A straw tube tracker consist of a series of what are essentially drift chambers. In general a drift chamber consists of an enclosure containing an anode and cathode separated by a region containing a gas. Ref. [12]?? The straws in the detectors consist of aluminized tubes which are then filled with an argon ethane gas and have an anode wire consisting of gold

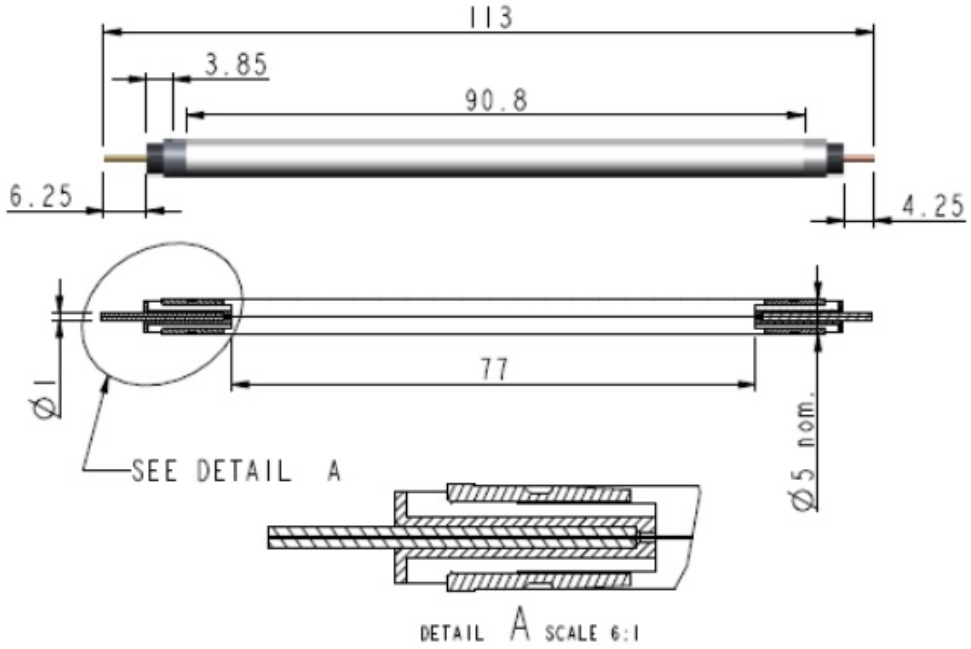

Figure 3.1: A Schematic showing the dimensions of a straw tube Ref. [12]

plated tungsten going through the middle of the straws. A diagram of the straw tube and its dimensions is found in Fig.3.1. For further information of the properties of the straws are given in Fig. 3.2.

As a particle passes through the straw the particle interacts interacts with the gas causing the ions to go to the cathode of the straw creating a detectable current. The ions are able to recover electrons from the cathode and the system and returns to a neutral state. This current can then be measured by the electronics designed for the experiment and can be given to the computer code which will extrapolate the decay position of the particle being detected in the experiment. For further improvement on spatial resolution, the amount of time for the ions to reach the cathode is dependent on where radially in the wire that the particle passes through, this is called the drift time. This drift time can then be extrapolated and added into the track fitting which an explanation of this will be in a later section.

Straw material	Aluminized Mylar
Straw wall thickness	15 μm
Wire	25 μm gold-plated tungsten
Straw length	10 cm
Stereo angle	$\pm$ 7.5° from vertical
Gas	50:50 Argon:Ethane
Pressure	1 Atm

Figure 3.2: A table show the properties of a straw Ref. [12]

One straw tracker consists of 128 of these straws which are each 5 mm in diameter. These 128 straws are then divided up into 4 layers which are oriented 7.5° off the vertical axis with two layers being in one direction off the vertical axis and the others layers are in the other direction. This 7.5° tilt of the straws allow for the tracking to take this into account an measure the vertical position that the particle hits the detector. This capability is especially important for the EDM measurement.

The next component of the straw tracker includes the manifold and the flobber. The straws are then connected to the manifolds which these allow gas to pass through them from one direction and out the other direction. In addition to this the manifold contains the cooling system and the first set of readout electronics. Attached to this manifold are two flanges referred to as the snouts which contain the electronic connections, the cooling system, and allows the gas to flow. Connected to these snouts is the flobber. The flobber houses the majority of the tracker electronics. A diagram of the tracker as a whole is found in Fig. 3.3.

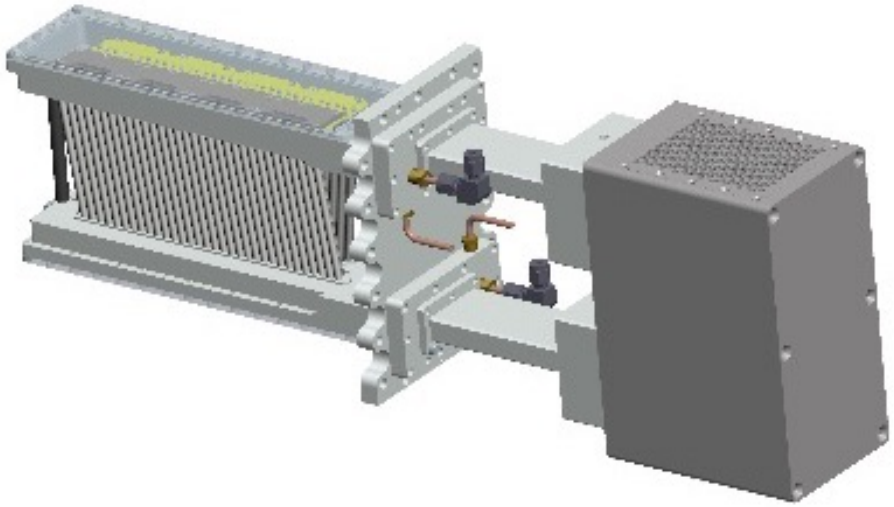

Figure 3.3: An example of a straw detector Ref. [4]

3.1.2 Hardware of the Straw Trackers

Now that the basic design, reasoning, and the terminology of the straw trackers themselves is established it is necessary for the systematic uncertainty discussion to give a basic introduction to the hardware that comprises the tracking system. In the tracker the straws are connected directly to the ASDQ's which is there to digitize the signal coming from the straw. Fig. 3.4 shows an image of one of these ASDQ boards. Every ASDQ board connects to sixteen straws so therefore there are eight ASDQ boards serving each tracker. Flexi-cables are attached directly to the top of the ASDQ boards and route the signal through the snouts to the flobber. A top view of the tracker showing the electronics can be found in Fig. 3.5 Inside the flobber the signal from the ASDQ boards is then passed to TDC motherboards. Each motherboard consists of two TDC's which connects to one ASDQ. The TDC boards

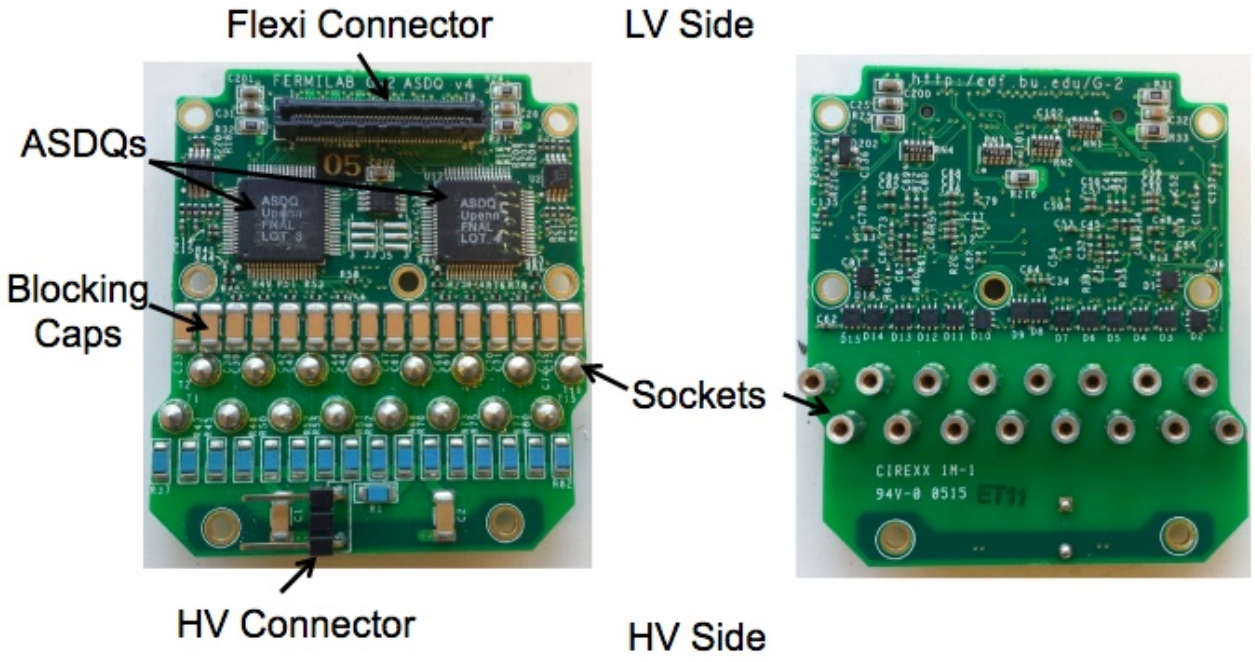

Figure 3.4: An example of a ASDQ board in the trackers Ref. [14]

buffer the signal before giving it to the logic boards. Each logic board takes the signal from two TDC's which means that there are four logic boards in a tracker. The logic boards serve as a further buffer for the data, control the clock, label the data, and incorporate data from the low voltage systems. The signal from the logic boards is then passed onto the external electronics located in the flobber.

The signal from the logic boards is passed to an FC7 board housed in an electronics rack and it serves to process the signals coming from the eight trackers at one station. Furthermore, the FC7 board controls the logic board clocks, converts the signal to a readable format for the next electronic board, and passes parts of the signal to a computer which can quickly identify data corruption. The FC7s communicate their data to AMC13 boards which control the clock of the FC7s and communicate the data to the data acquisition system. A single AMC13 can control all of the tracking stations.

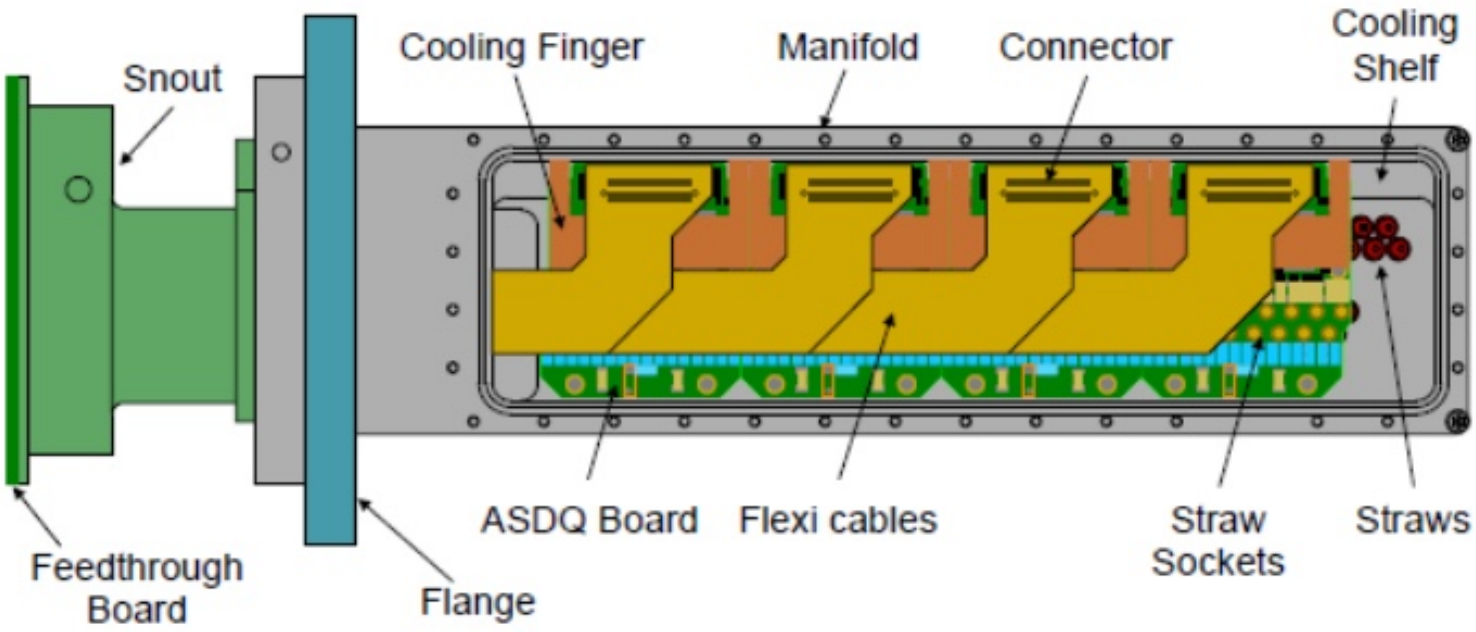

Figure 3.5: Cross Section Top View Showing Tracker Electronics Ref. [15]

3.2 Straw Tube Tracking Algorithms

An important part in evaluating the systematic uncertainties of the straw tube tracking is to understand what the tracking algorithm consists of and how the track fitting process works. In addition, in this section will be an explanation of the data products, what the components of the data products used physically mean, and how those data products are then derived from the tracker data.

3.2.1 Introduction to the Straw Tube Track Finding

For each process that the tracking algorithm follows it uses what is called an Art module. Art is an event processing framework used in particle physics.[16] Art is C++ framework that

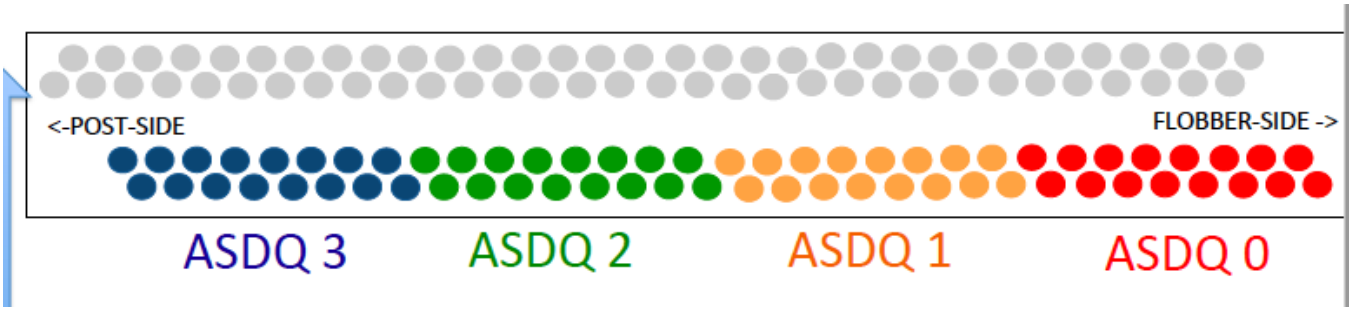

Figure 3.6: Illustration that shows how the channel ID's are split up for each wire. Ref. [17]

allows different components of code to be used interchangeably, as long as the appropriate data products are being used. This is the main framework for the whole project and all the code that is discussed further is written in this framework.

The straw tube track finding algorithm consists of the most processing steps in analyzing the data. Although, more complicated and robust than what will be presented the basic idea of the tracking finding and fitting is covered. From the electronics the computer collects the data and makes compressed data file. For tracking these files only consist of raw Digits. These raw digits contain all the information that will be used further in the code and consists of the timing, and where the signal comes from in the electronics. How the channel ID's are split up can be found in Fig. 3.6. Each channel corresponds to the same ASDQ and the same logic board. Every station has the same AMC13 ID. There are two TDC's per channel which one TDC would correspond to one layer in a channel. Furthermore, this data product contains the width. The width that is the time difference between the rising edge in the wire when current is above a threshold and the falling edge where the current falls below the threshold.

From this raw data there is a module the makes a more user friendly data product called straw digits. From the raw digits, and a geometry file converts the ID's to the specific 3d coordinate where the wire is positioned. In addition, from these Raw Digit ID's there is

generated a wire ID, which gives an easier format to label wires. The wire ID gives the particular wire that was hit and tells what station, tracker, layer, view, and wire position of the hit. The convention for number these value goes as follows, there are two stations 12 and 18, there are 8 trackers per station which the lowest number is labeled closest to the ring, there are 2 layers (0,1) looking at Fig. 3.6 the first layer is 0 and the second layer is 1, the third layer is 0 and the fourth layer is 1. There are 2 views in a tracker (0,1) which this corresponds to u or v layer respectively. The wires are labeled from 0-31 with the lowest number being the side that is closest to the beam. Lastly this module, also calibrates the TDC times so that they are all in time with one another. Lastly, in the straw digits there consists several other parameters created in this module although they are just filled in as empty to be used later in the code consists of the drift time, error on the drift time, reconstructed distance of closes approach, and the distance of closest approach error. I will explain these additional parameter later when these parameters are filled with data in the code.

From the straw digits the next module in the algorithm splits these straw digits into 100 ns time intervals which are called time islands in order to make the straw digits more manageable. Typically these time island consist between one and four tracks. In addition, this module also extracts what is called the t0, which is the time at which the track hits the first straw in the detector. The t0 has multiple different calculation methods. However, it has been found that the best working method for calculation is the average time method where you take the average between the minimum time and the maximum time found in the time island. This value is then adjusted to extrapolate back to where the tracks hits the first layer, telling you at what time the track hits the detector. The time islands data product consists of a unique island ID, the mean time, minimum time, maximum time, t0, t0 algorithm ID, t0 success, and the station where the time island occurs. In addition to

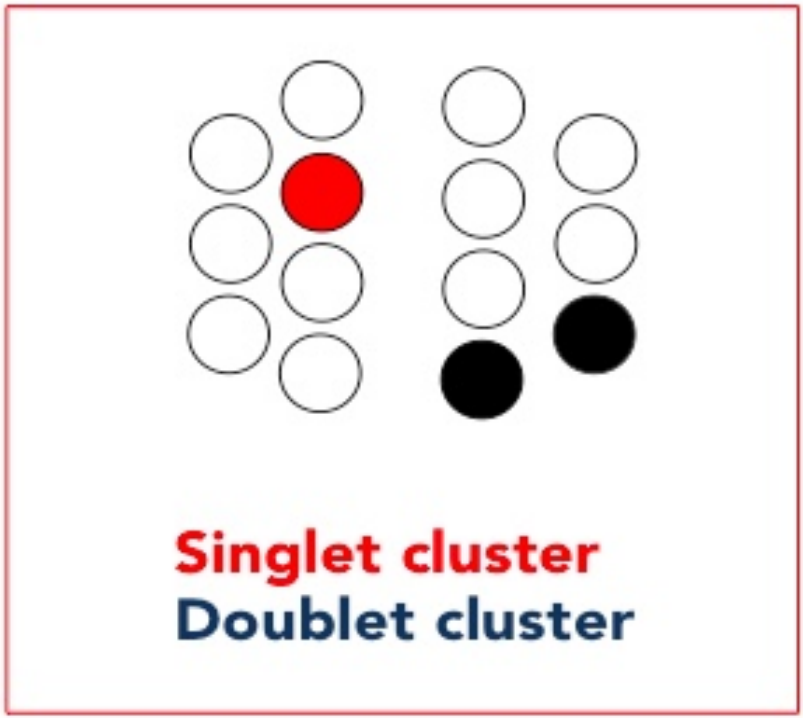

Figure 3.7: Examples of Clusters. Ref. [18]

this, there is a parameter called the upstream digit which stores the wire id of the wire used in the t0 calculation.

Next, the time islands are then passed onto the clustering module which groups the digits in the time islands by digits that are neighbor each other. In addition to this from the UV angles and the geometry of the detectors the horizontal position of the track is measured. An example of a cluster pictorially is shown in Fig. 3.7 . This data product that is passed on has the following parameters to use: mean time, t0 (initial time of cluster), t0 error, the coordinate position of the cluster, horizontal position, horizontal position error, the station number, module, view, and tells if the clusters either overlap with another cluster or if they have shared digits between the cluster. This information is useful for the next module in the process.

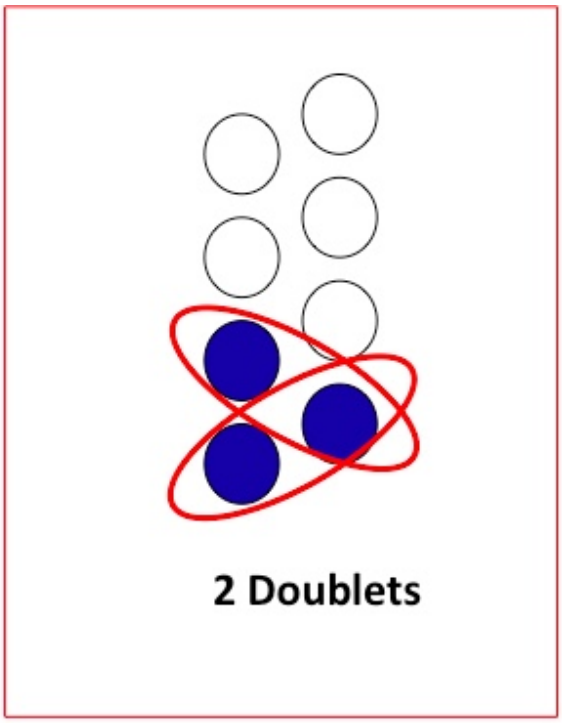

Figure 3.8: An example of two neighboring seeds from one cluster. Ref. [18]

The clusters of digits are then processed by the next module which forms what are called seeds. Seeds are derived from clusters which give possible combinations of digits in a particular layer that would belong to a track, ie. a track is composed of a multitude of seeds. Fig. 3.8 Is a good example of how a cluster could form two seeds. The information that is given then from this module consists of: The type of seed (how many seeds belong to that cluster), time , 3d coordinate of the seed, the line slope of the digits on the seed, the line intercept of digits on the seed, if it has shared clusters, station, and whether the first digit is in the front view or the back view.

Probably the most complicated part of the code consists of the next module where this forms track candidates. A track candidates is a single particle track that is derived from the seeds previously established. This is a fairly robust program that can pick out multiple tracks in a time island and forms every possible combination of the seeds a picks out which

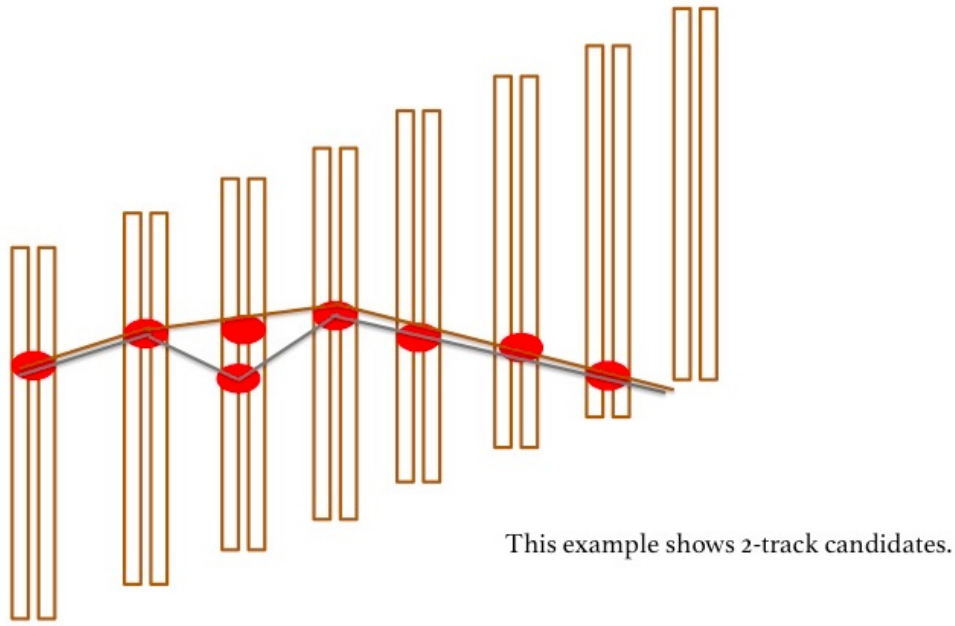

Figure 3.9: An example of how a track candidates would be formed. Ref. [18]

combinations make physical sense. Shown in Fig. 3.9 would explain how this algorithm forms different track candidates.

Now that the track candidates are created it is necessary to derive the track t0, drift time, and to reconstruct the distance of closest approach. Similar to finding the t0 in the time island, the t0 is calculated by finding the average time from the first digit and the last digit in the track candidate and then extrapolating to the time that the first digit in time hits the track. The t0 is an important component to determining the drift time of the straw digit and therefore the distance of closest approach. The drift time of the straw hit is determined as the difference between the hit time of the straw (which is the average time between rising and falling edge of the current) and the t0. Refer to Fig. 3.10. An example drift time distribution that is normally seen is found in Fig. 3.11 From this drift time now can be determined the distance of closest approach. The distance of closest approach is determined

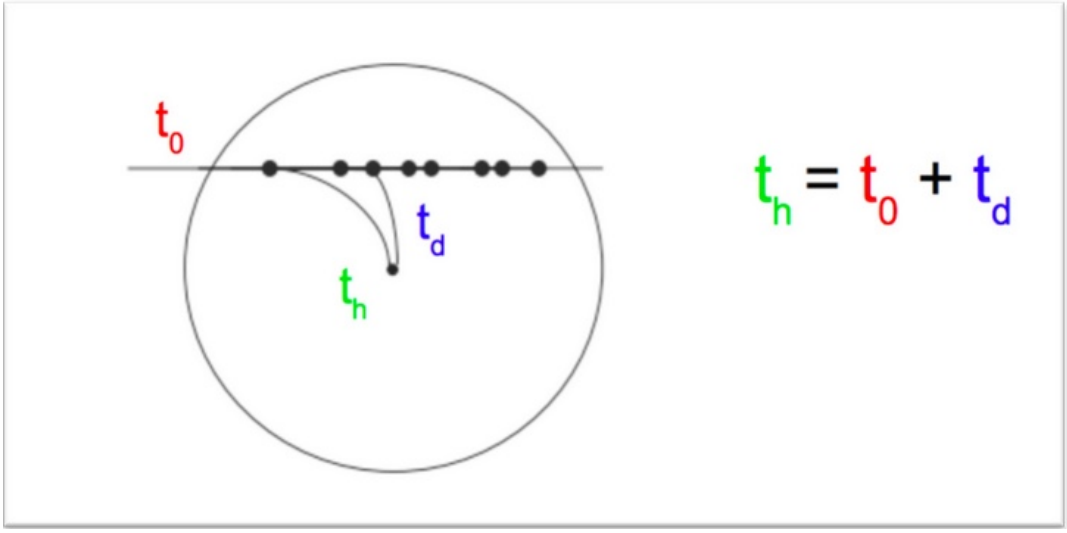

Figure 3.10: This shows how the drift time distribution by the given t0 and Hit Time Ref. [18]

from a physical model that was determined from Ref.[20]. From an experimental method a 2d histogram of drift time vs. the distance of closest approach (from the track fitting algorithm not explained yet) as shown in Fig. 3.12. In Ref.[20] he produced a histogram by splitting it up in several regions dependent on the distance of closest approach. Then these functions were fitted with a gaussian convoluted with an exponential. Then generated was the mean value of the drift time versus the distance of closest approach. This model then directly converts a drift time to a distance of closest approach with some uncertainty.

3.2.2 Track Fitting and Reconstruction

The track fitting and the track reconstruction is a complicated process that will be explained briefly. The fitting algorithm used is a standard χ^2 fitting algorithm where there is a starting $\vec{p}$ and then the χ^2 value is minimized to the data. In order to do the fit it is necessary to determine whether the track goes to the left or right of each wire. This

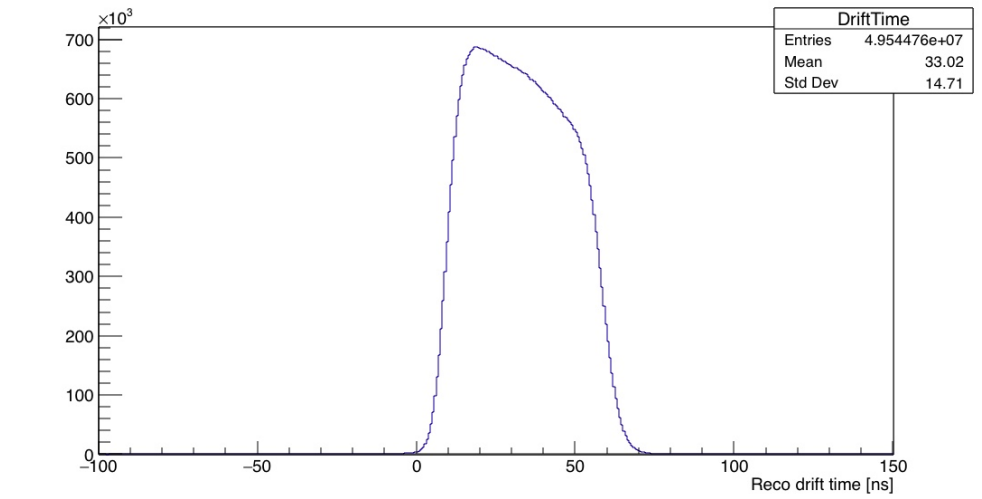

Figure 3.11: This show what a typical drift time distribution looks like

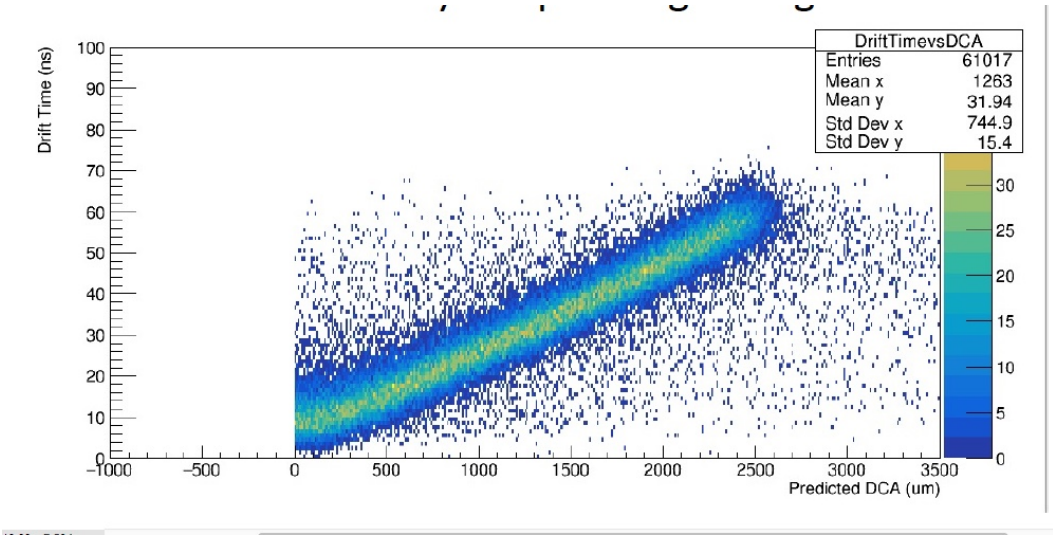

Figure 3.12: Example histogram of how the distance of closest approach is modeled

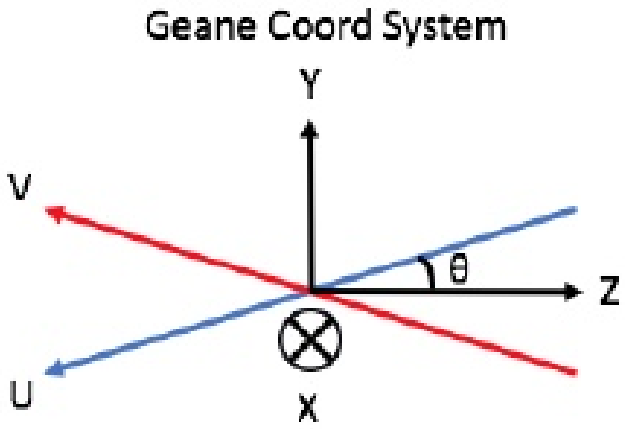

Figure 3.13: How the xy coordinates system relates to uv coodinates system, z is in direction of the trackers, x is parallel to the tracking planes, z is horizontal Ref.[**?**]

is handled by first doing a simple linear fitter between seeds that are doublets. For each doublet the algorithm goes between every different combination of left and right sides of the wire. Then the angle between the lines between neighboring seeds are minimized to one another and those selections of left or right side of the wire is chosen. Now there is a five parameter χ^2 fit described by the variables $(\frac{1}{p}, \lambda, \phi, y_\perp, z_\perp)$.The variable are then transformed using a Jacobian to $(\frac{1}{p}, \frac{pu}{px}, \frac{pv}{px}, u, v)$. Then they can be converted from uv coordinates to xy coordinates using another Jacobian. [**?**]. Fig.3.13 describes how the uv coordinates are related to the xy coordinates in the fitting.

The track extrapolation algorithm uses a Runge-Kutta Nystron algorithm. The algorithm begins with a state vector $\mathbf{S}_i$, positions and momentum of the fitted track. These parameters are propagated along a step $\mathbf{d}_o$ by evaluating the equation of motion at four immediate stages. The magnetic field information is queried back at each one of these stages. The angles of the track at each stage are weighted to obtain the final state vector at the end of the step. Refer to Fig. 3.14 for a pictorial representation. After each step the geometry of the ring is queried and flags each track that hits a material in the ring. Also at each step the radial

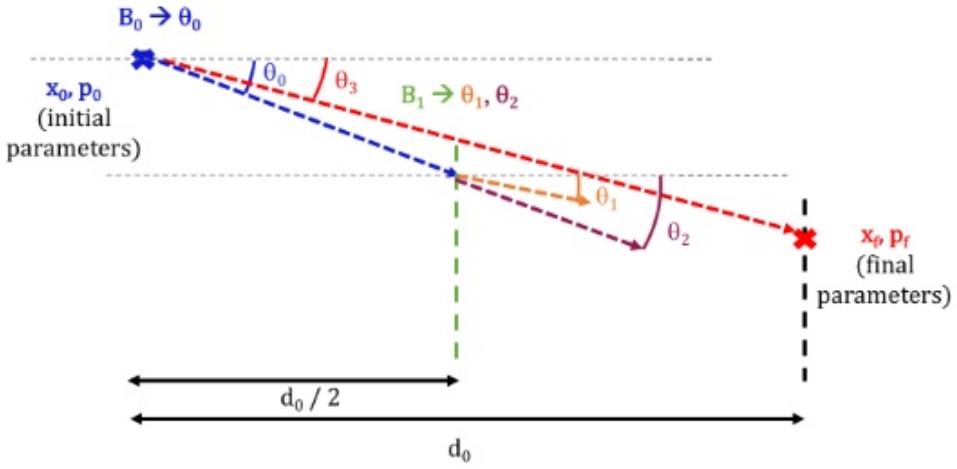

Figure 3.14: A pictorial explanation of an extrapolation step [22]

momentum component is evaluated and the extrapolation stops when the radial momentum is zero or in other words when the extrapolated track is parallel with the storage ring.

3.3 Uncertainties in the Straw Tube Detectors

After the tracking methods have been established it was necessary to understand exactly where the uncertainties are coming from and how much they contribute to the final measurements.

3.3.1 Explanation of Uncertainties

Uncertainties are an important aspect of the gm2 experiment. Significant care has to be taken to ensure that we do not have more than the budgeted errors established in previous sections in any section of the experiment or the experiment will not succeed. Therefore, since the development of the trackers and the tracking algorithms the tracking team has

spent a significant amount of time trying to address and characterize different systematical error that may happen in the experiment. This section gives a brief explanation of the errors that are associated with specifically the tracking analysis mainly done by collaborators.

As shown before the main ability of the trackers is to have good spatial resolution as compared to the calorimeters. Therefore, in studying the systematics the main extrapolated quantities of interest is the extrapolated y position (horizontal position) and the radial position (decay point in the ring). All of the important quantities for the experiment that are on a tight error budget are derived from these quantities. Furthermore, for brevity I am only going to cover the final errors contributed to the pitch correction and the electric field correction which use the y and r position respectively.

For the pitch correction refer to Table 3.1. The single largest error is from the acceptance effects of the trackers which consists of 16 ppb which is larger than all the other systematics being discussed. Looking at the largest error found in Table 3.1 which is the straw stereo angle this will be deviation of the straws from the idealistic 7.5°. On a similar scale of this error is the ability to find the Left and Right side of the wire in the track fitting. The next largest error consists Lost muon contamination which are muons hitting the detectors that never decayed into a positron. Internal alignment is the deviation of the individual straw trackers from the idealistic geometry. Close to this is our ability to determine the t0 of the track which was explained previously.

The following errors contribute all on the same level. Then the hit resolution which will be explain in a later section. The external alignment which is the deviation of the tracker station as a whole from the ideal geometry. The track finding errors are from when we pick the wrong track candidate or a wrong digit. Material effects are from ignoring the fact that the positron is passing through a mylar straw. Lastly, the smallest contribution is the contribution from electronic cross talk which will be discussed in a later section.The other errors we know are there however they have not been currently determined. This consists of

Table 3.1: Systematic Error Contribution of the Pitch Correction

Systematical Error	Error (ppb)
Stereo Angle	6.9
L/R	6.9
Lost Muon Contamination	2.9
Internal Alignment	1.5
t0	0.6
Hit Resolution	0.3
External Alignment	0.3
Track Finding	0.3
Material Effects	0.3
R to T	?
Magnetic Fringe Field	?
Cross-Talk	<0.005

variances in the magnetic fringe field near the trackers since this is a derived quantity not a measured quantity. The R to T error is the error being introduced from our distance of closest approach and drift time model variations. [23]

In conclusion currently for the pitch correction the total systematic uncertainty 19.3+?. For the 60 hour data set the tracker it is found that the measured pitch correction is given by $C_p = 164.7 \pm 0.1(stat) \pm 21.1+?(syst)$. Although a bit large for the total error budget of 30 ppb for both the E-feild and pitch corrections this is only the first run in the experiment and in the future a lot of these systematics will get much smaller. There is no need to discuss the radial parameter it given in a little different format actual error vs. ppm but you still can get the general idea of how much different aspect contribute. Here it looks like the internal alignment is the greatest contributor to the errors of the electric field contribution. Refer to Fig.3.2

Table 3.2: Systematic Error Contribution to Radial Disribution

Systematical Error	Error (mm)
Stereo Angle	?
L/R	0.2
Lost Muon Contamination	0.055
Internal Alignment	0.162
t0	0.035
Hit Resolution	0.03
External Alignment	0.01
Track Finding	0.03
Material Effects	0.02
R to T	0.026
Magnetic Fringe Field	?
Cross-Talk	<0.005

CHAPTER 4

STRAW TUBE TRACKER SYSTEMATICS

With the straw tube trackers being an important part to the EDM measurement it is important that the systematics of the system are fully investigated and understood as to minimize the errors in the pitch correction, beam dynamics, and electric field corrections, along with the EDM and MDM measurement. This chapter will explain the particular errors of cross talk and hit resolution in the straw detectors and how these errors were characterized and there relative effect on the measurements.

4.1 Cross Talk in the Straw Trackers

Cross Talk is an effect when there is a particle signal in one wire which causes a signal in another wire. This could be catastrophic for the measurement especially in the pitch correction and the EDM measurement as this would throw off the extrapolated y position due to the bias in the track fitting. Furthermore, If I add in another hit in a straw when there is not supposed to be a hit then this could either shift the particular y position at a plane and cause an error in the fit or an extra deviation in the fitting algorithm. Please refer to figure **??** If we have a digit that occurs at position 1 and 2 this could show that the particle trajectory is in the $+y$ direction, alternatively if we get a digit that occurs in position 1 and 3 this would show the particle trajectory would be moving in the $-y$ direction directly throwing of the results for this measurement. This section will explain the process

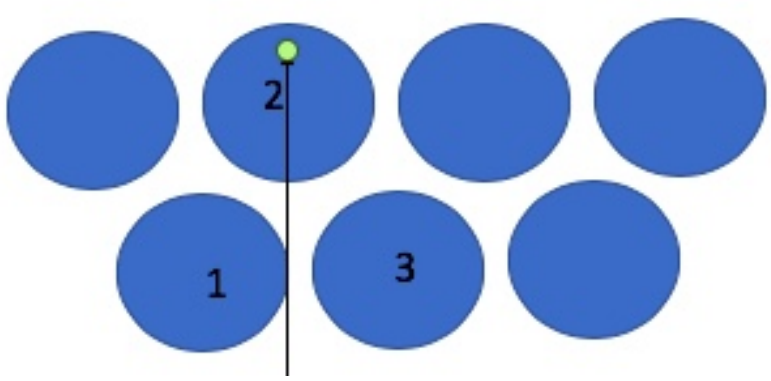

Figure 4.1: A pictorial representation of how Cross Talk was picked out

how I characterized and then added this effect into simulation as to see how much of an effect this will cause and our extrapolation y positions and radial positions in the detector.

CrossTalkEval.jpeg

4.1.1 General Explanation of Cross Talk

Cross talk, or what we are calling cross talk, in the detectors could be caused by multiple different processes in the detector. Firstly, because the mylar tubes as explained in the previous section are conductive and these tubes are neighboring each other this could create kind of a capacitor that holds charge and discharges onto the neighboring wires creating a false signal in the detectors. The next source of cross talk in the detector could be from within the electronic boards themselves. When traces on a printed circuit boards are neighboring similarly this could create an inductive or capacitive couple between the traces causes a signal from one trace to bleed into another trace. It is unknown which of these are the greatest effect but they should have similar properties and this is what we would consider cross talk in the detectors. Thirdly, although not technically cross talk we could have a case when there is a muon in the detectors and it decays to a positron therefore causing a

signal in another wire and confusing the tracking results. All of these properties are lumped together further in this analysis since it was just needed to evaluate the properties of these effects and add it into simulation as to see the effect on our tracking finding and our final tracking fitting results.

4.1.2 Evaluation of the properties of Cross Talk

In order to add the effects of cross talk into the simulation and to understand the true effects that cross talk has on our track finding and fitting we needed to ask the questions when does cross talk occur after the first digit, is there any correlations between the data products of the cross talk hit or the primary hit (The hit that causes the cross talk), how much cross talk occurs in our detectors...etc. To do this it is necessary to establish the know properties of cross talk just from the very definition of it being cross talk. Firstly, we know that cross talk is caused by something else so it has to occur after another hit in the detector. Secondly, we know that from the sources of cross talk established earlier we are most likely going to find cross talk in the neighboring wire. Lastly, since the cross talk signal again is caused by charge in another wire the primary signal charge cannot be larger than the cross talk signal charge. These properties will be important for selecting out particular tracks and will allow us to pick out cross talk signals.

Firstly, it was necessary to get a known cross talk sample. To get these known cross talk signals we looked at a particular case where there is only 1 particle that was going through the detector at a time. The next criterion that was necessary is that we required there to be 2 hits in the same layer of the detector without any hits being in the opposing layer. The next criterion that is required, as to take out the case of decaying muon in the detector, there is a momentum cut at 2300MeV so that we know that there are minimal muons in the

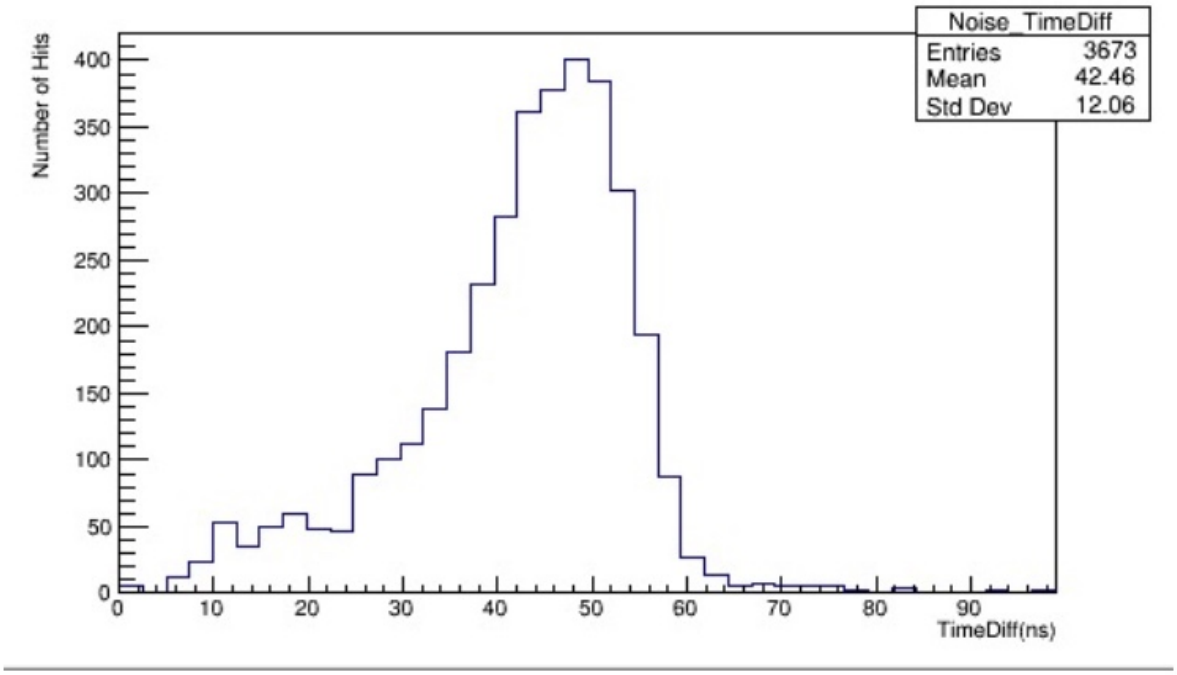

Figure 4.2: The observed cross talk time difference distribution from data at 1550V.

detector so there is only the case of electronic cross talk. Now we only have the case where there is a primary digit and a cross talk digit, with the primary digit occurring first in time. The time distribution between the primary digit and the cross talk digit is found in Fig. 4.2, which has an odd shape mainly due to the fact that there are multiple different situations of cross talk occurring. Next, if we look at the drift time distribution for cross talk, found in Fig. 4.3, it is shown that generally the drift time for cross talk is fairly large. Furthermore, looking at the distance of closest approach distribution of cross talk Fig. 4.4 , due to the large drift time, results in most of the cross talk looking like a particle hit on the edge of the wire.

Next it was necessary to evaluate the general properties of cross talk, they are not necessarily important for the simulation; However, it is nice to know and document the properties as a quality control standard. In addition, this gives a good double check that the previous

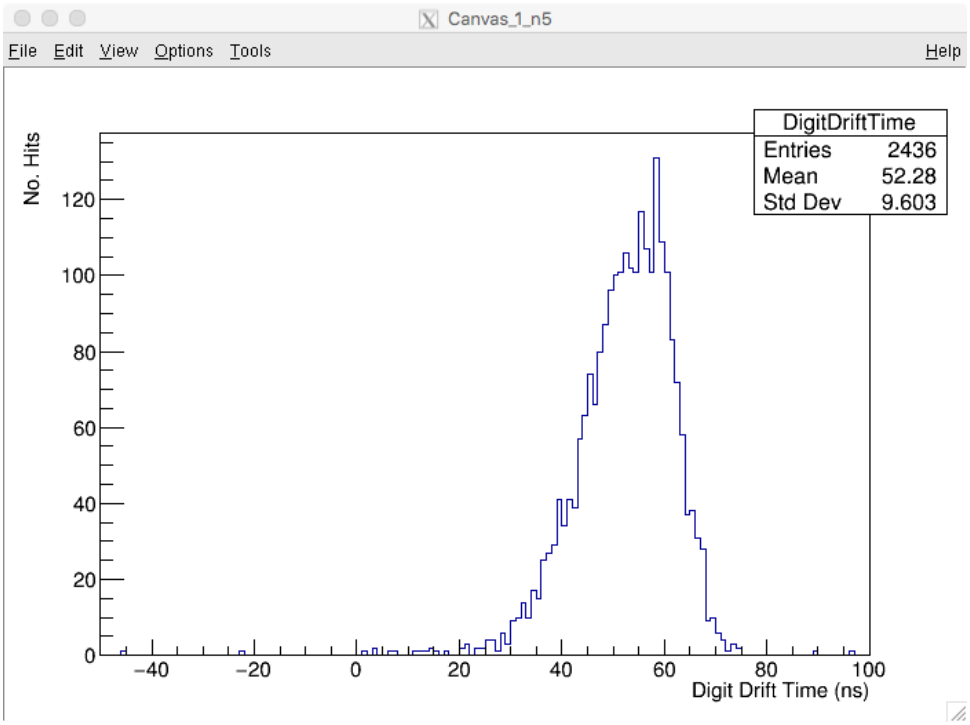

Figure 4.3: The observed cross talk drift time distribution from data at 1550V.

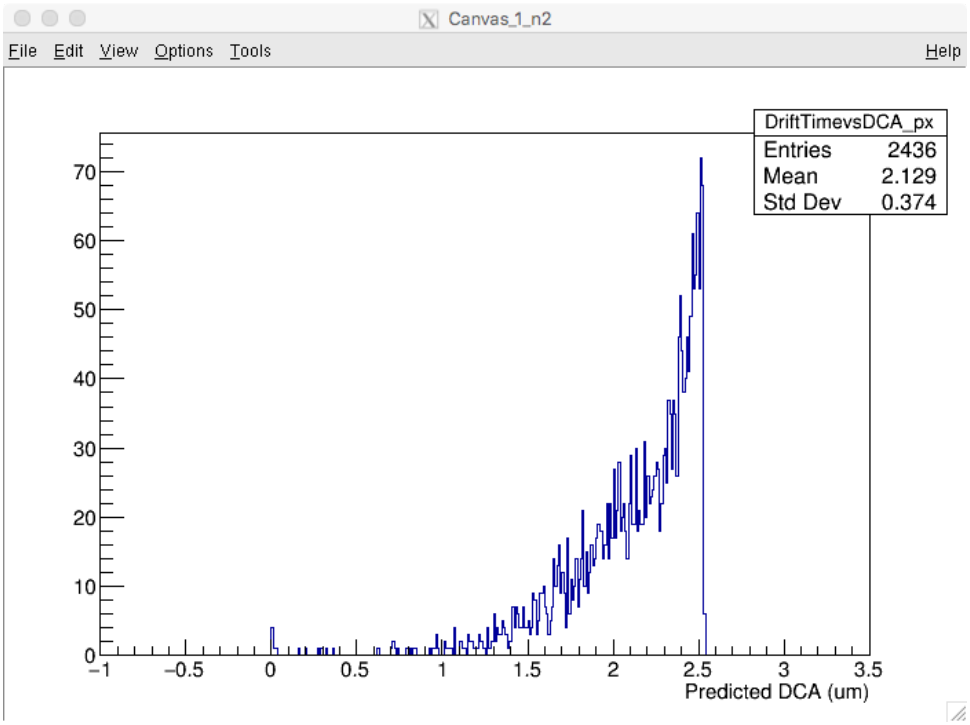

Figure 4.4: The observed distance of closest approach distribution from data at 1550V.

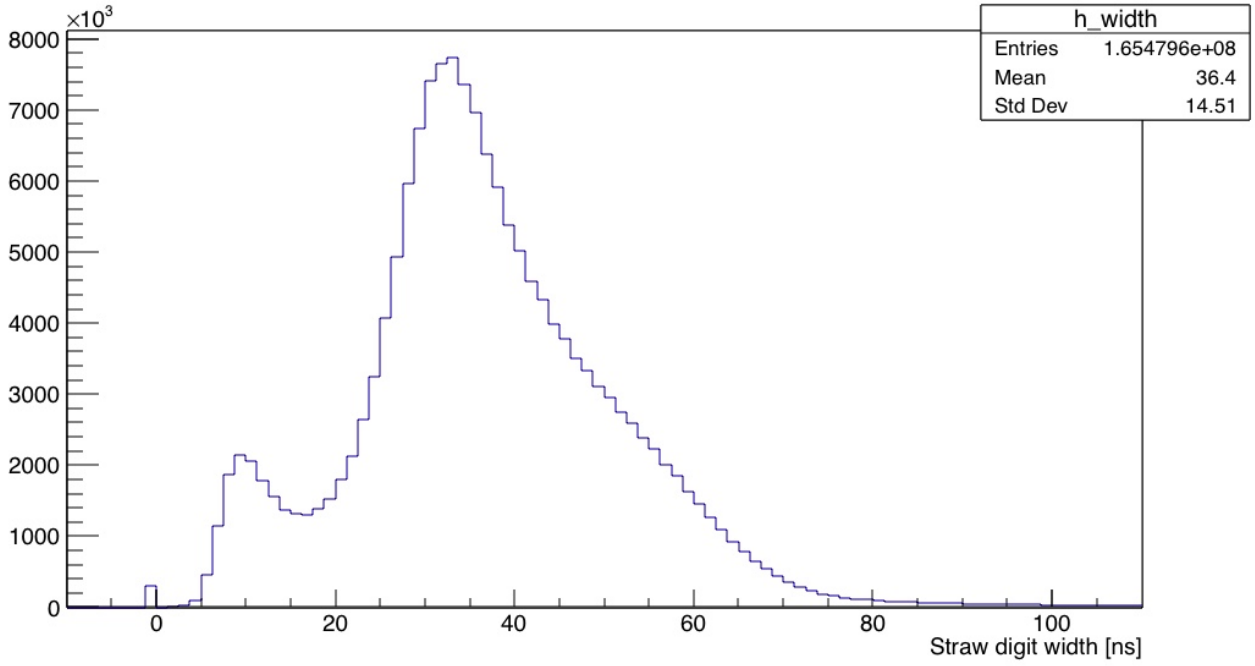

Figure 4.5: The Normal Hit width distribution without track selection

method of establishing the properties of cross talk are valid. It was found that the hit width distribution, which was explained previously in the tracking section, had an odd shape with one little hump on the small hit width side and a large overlaying hump as shown in Fig. 4.5. It seems that this would be the cross talk since we would expect the cross talk signal to be small, at least smaller than the primary digit. To prove this I used the previous method to select out cross talk and the primaries. Putting these into the hit width distribution Fig. 4.6 I found that the assumption that digits that are larger are more likely to cause cross talk digits that are small is valid.

The cross talk in the detector should be dependent on the gain in the straws and therefore the cross talk will be dependent on external weather effects due to the properties of the argon ethane gas changing. To investigate this I looked at data on a data set which was ran over 60 hours, averaged the temperatures and pressures over the series of runs, and looked at the

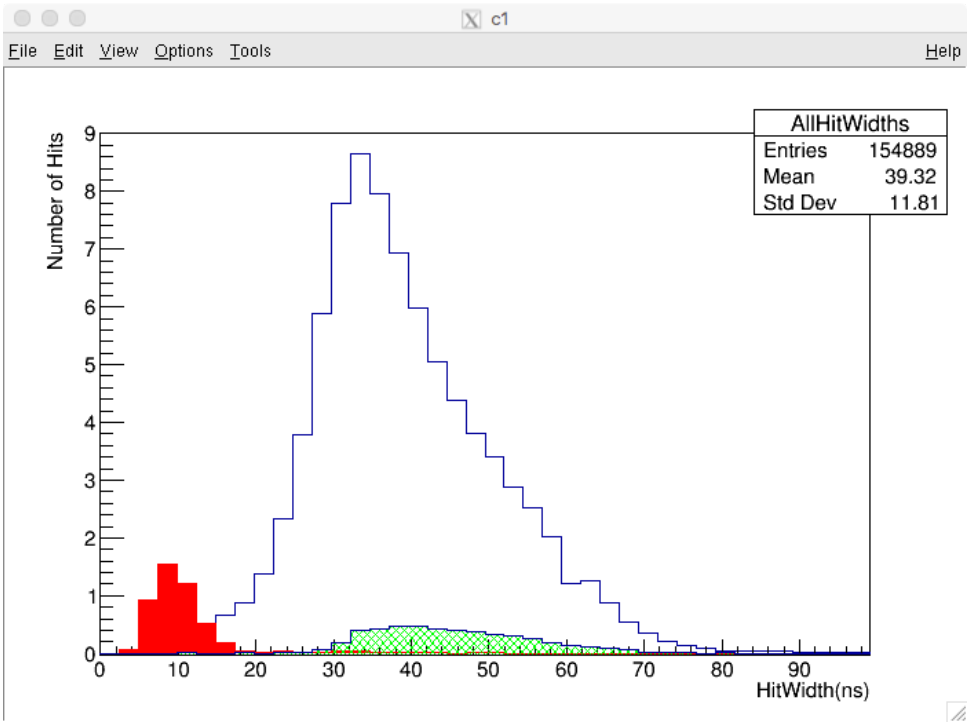

Figure 4.6: The Normal Hit width distribution overlaid with primary digits

number of cross talk digits vs. the number of tracks found in that layer. Fig. 4.7 shows how the cross talk increases as a function of temperature and Fig. 4.8 shows how the cross talk I selected decreases as a function of pressure. These results are consistent with what I would expect with cross talk. In Fig. 4.9 shows how the cross talk varied over multiple detectors over that same 60 hour period which shows that there is a fairly large variance in cross talk from run to run. Note, the percentage on the y-axis is arbitrary since its the percentage of tracks, the point of these is to confirm that the properties of the digits I collected as cross talk have the properties of cross talk. As another double check, the gain is also dependent on the voltage on the trackers. Therefore, we should expect that the cross talk vs. voltage should give an exponential curve until we get to saturation. In Fig. 4.10 shows how the gain is dependent on the voltage. Using data from different voltages in the detectors it is found that this is true given in Fig. 4.11.

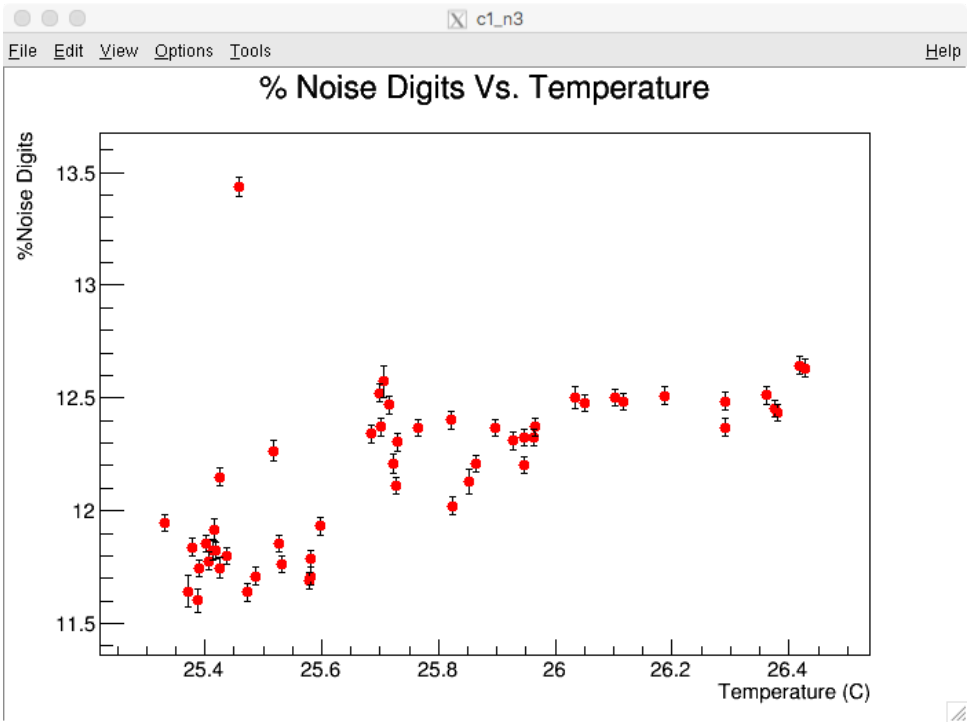

Figure 4.7: The observed correlation between cross talk and temperature. Note: Not true cross talk probability.

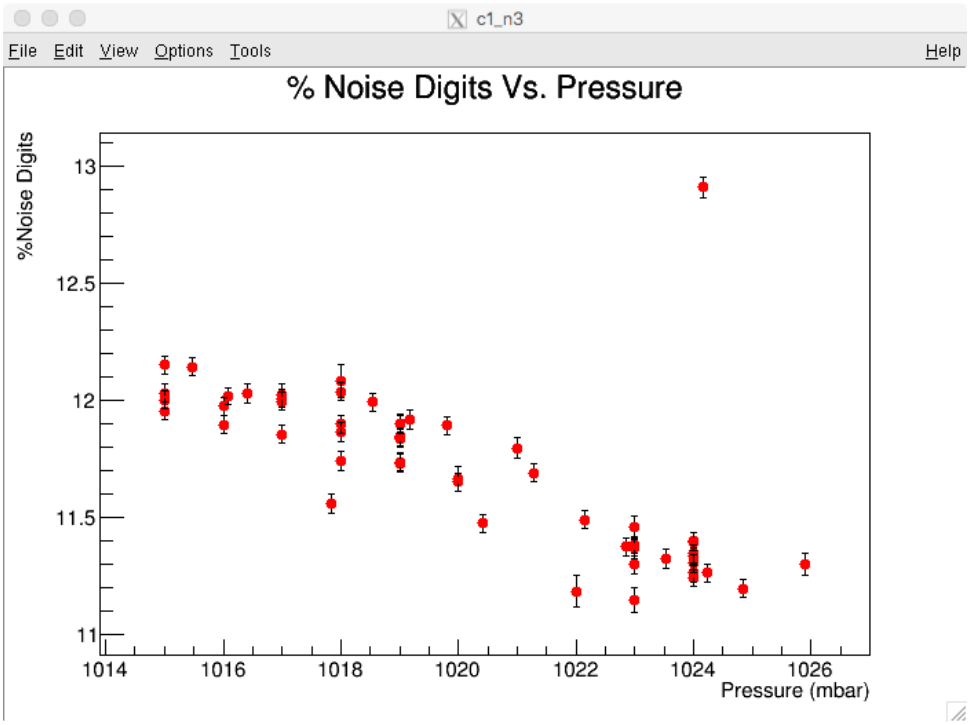

Figure 4.8: The observed correlation between cross talk and Pressure. Note: Not true cross talk probability.

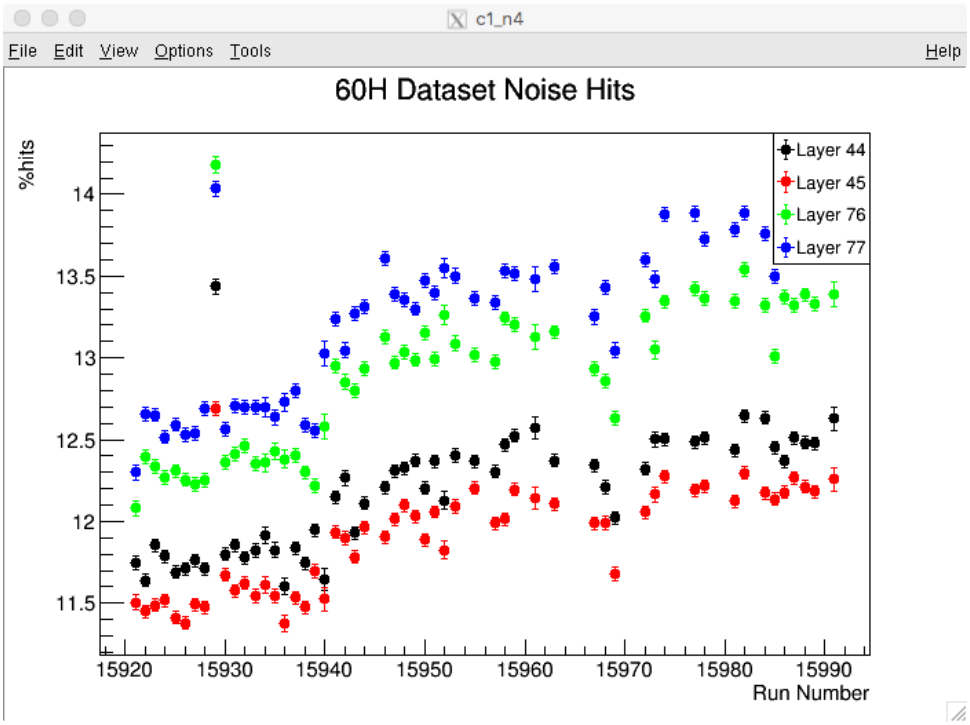

Figure 4.9: The observed correlation between cross talk over the course of time. Note: Not true cross talk probability.

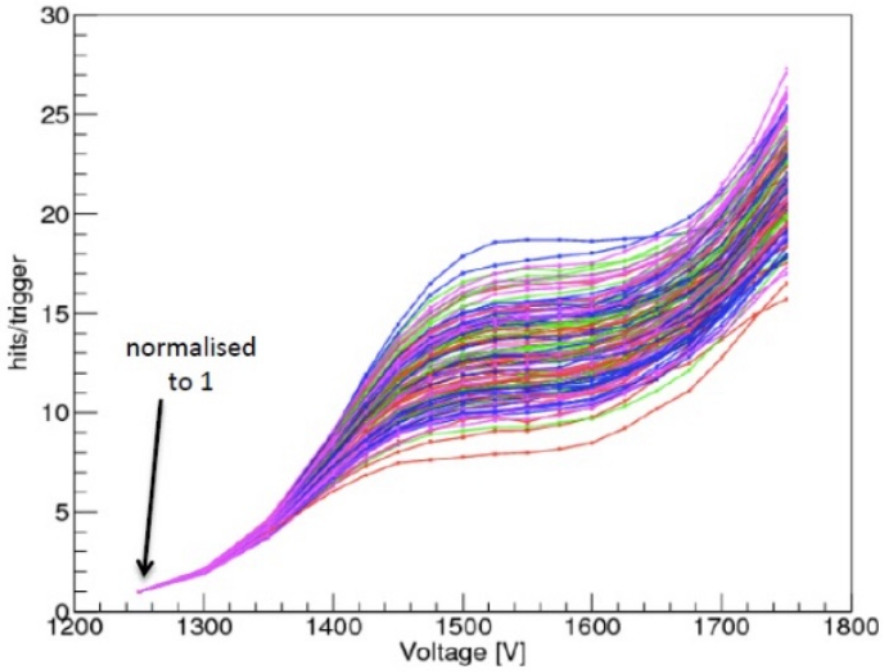

Figure 4.10: The plateau plot of 32 straws in the straw tracker. Y axis is essentially proportional to gain.

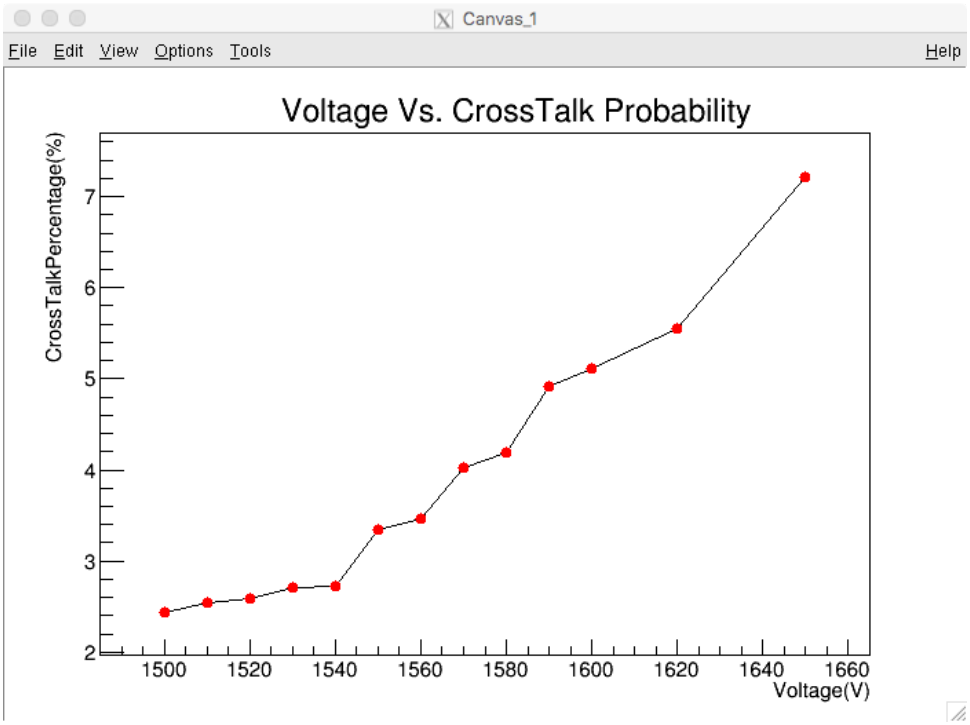

Figure 4.11: The observed correlation between cross talk with voltage. Note: Not true cross talk probability.

4.1.3 Introduction of Cross Talk into Simulation

Now that the properties of known cross talk signals and the signal the causes the cross talk are characterized it is now necessary to add the cross talk into a simulation to observe the effects that the cross talk has on the tracking. Firstly, it is necessary to establish at which step it is required we add in the cross talk and what properties are required so that we can randomly add this into the data.

In order to explain the reasoning behind this step it is necessary to explain a little bit about how the simulation that is being used works and what is being added in for data along the way. The simulation that we used is what is called a gas gun simulation where particles are randomly positioned in the ring at there decay points with some initial momentum defined by the simulation. The particle then decays to anywhere in the ring and then we can look at the decays that hit the detectors. The next step then picks out the specific straws that are hit and the distance from the center of the straw and then creates the digits. These digits only have the properties of what is called the wire id, which just labels the specific straw that is hit, and the time at which the wire was hit. Then the tracking algorithm uses this data to do the normal tracking algorithm that is established in previous sections. With this being said it was found that the best place to add in the effect of cross talk is just after the digits for the actual track are being added in since we need the properties of those particular digits, such as where the cross talk digits will occur and at what time the digits will occur.

To add the effect of cross talk into the simulation I randomly pick some digits that are generated in the simulation according to a defined percentage which is defined as a variable in my code. Then added in is another digit into the neighboring wire to the random time distribution that was found Fig. 4.12. Next, regenerate all the digits with the cross talk digits

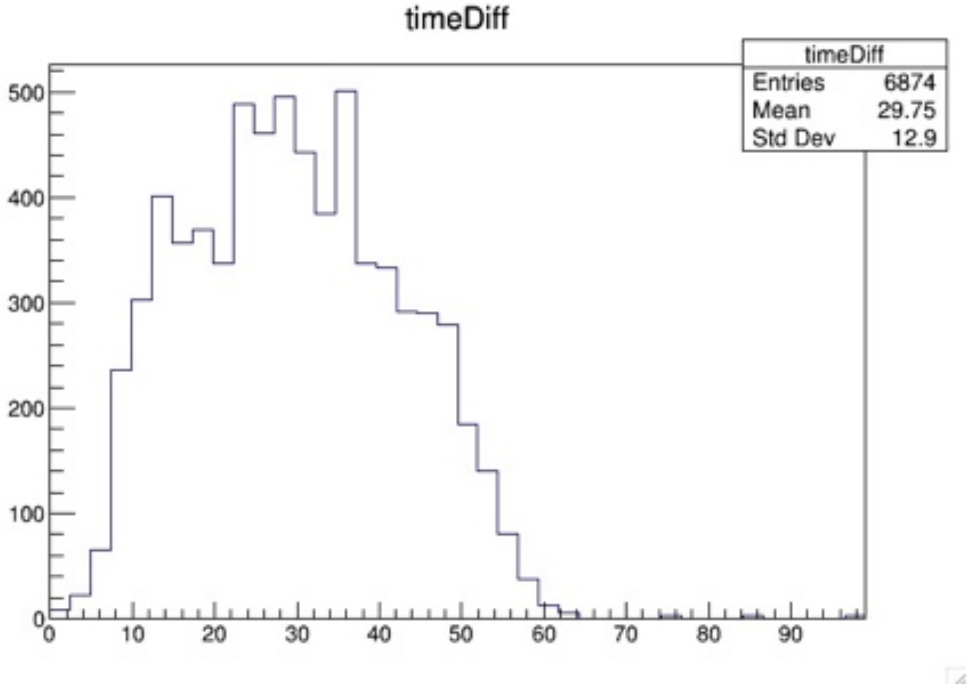

Figure 4.12: The time distribution of simulation

and pass it on to the next section will be the tracking algorithm defined in previous sections. To confirm that the coding was right it is satisfactory to look at the time distribution as given in the simulation, since this is the only defined parameter in the code, this is found in Fig.4.2 . This shows that the data and the mathematical model agree so therefore confirmed that the programming was correct in the simulation.

Comparing the vertical positions and the radial positions for different cross talk probabilities found in Fig. 4.13 and Fig. 4.14respectively. Here the black is 10,% red is 25% ,green is 25%, and Blue is 100%. These plots show that for a significant amount of data that the cross talk will not have a significant effect on the vertical or radial distributions. However, I need to get a number for error associated with the cross talk probability and we know it is not zero. Furthermore, it is necessary to find out how many tracks are effected by the cross talk and specifically how the cross talk effects the extrapolated vertical and

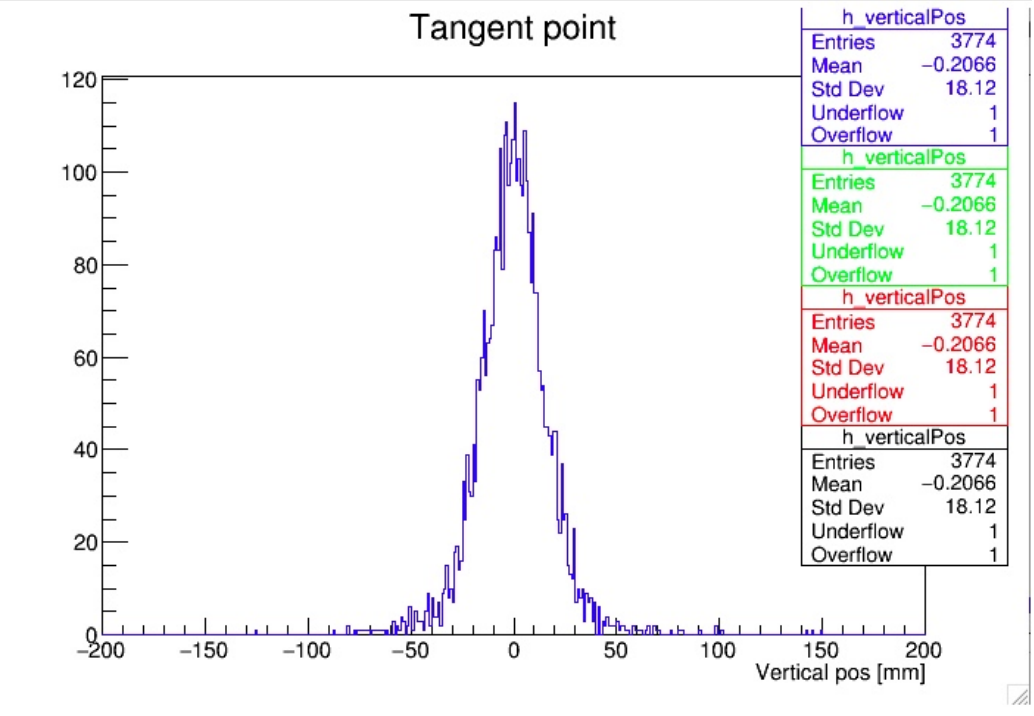

Figure 4.13: Comparison of vertical Distribution with different amount of cross talk 10% (black) 25%(Red) 50%(Green) 100%(Blue)

radial positions. 4.15 and shows the percentage of tracks with cross talk found in them vs. the cross talk probability. Here the y axis is in percentage of tracks which shows that only 0.5% of the tracks make it past the track finding algorithm which shows how robust this algorithm is. Fig.4.16 shows the difference between a track with and without cross talk for the vertical distribution. Using these numbers of the standard deviations and the means and the percentage of these tracks that are found in the final data gives an error of $< 0.005mm$.

4.2 Hit Resolution in the Straw Trackers

Hit resolution in the straw trackers is the spatial resolution at which we are able to determine the distance of closest approach to the wire in question from the found drift time

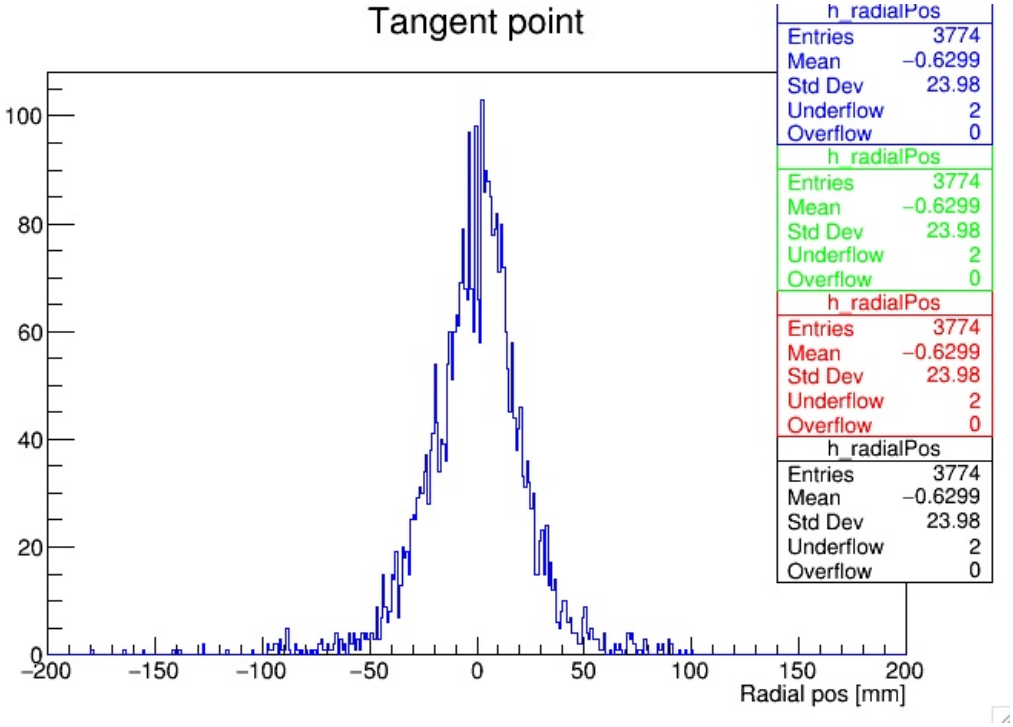

Figure 4.14: Comparison of radial Distribution with different amount of cross talk 10% (black) 25%(Red) 50%(Green) 100%(Blue)

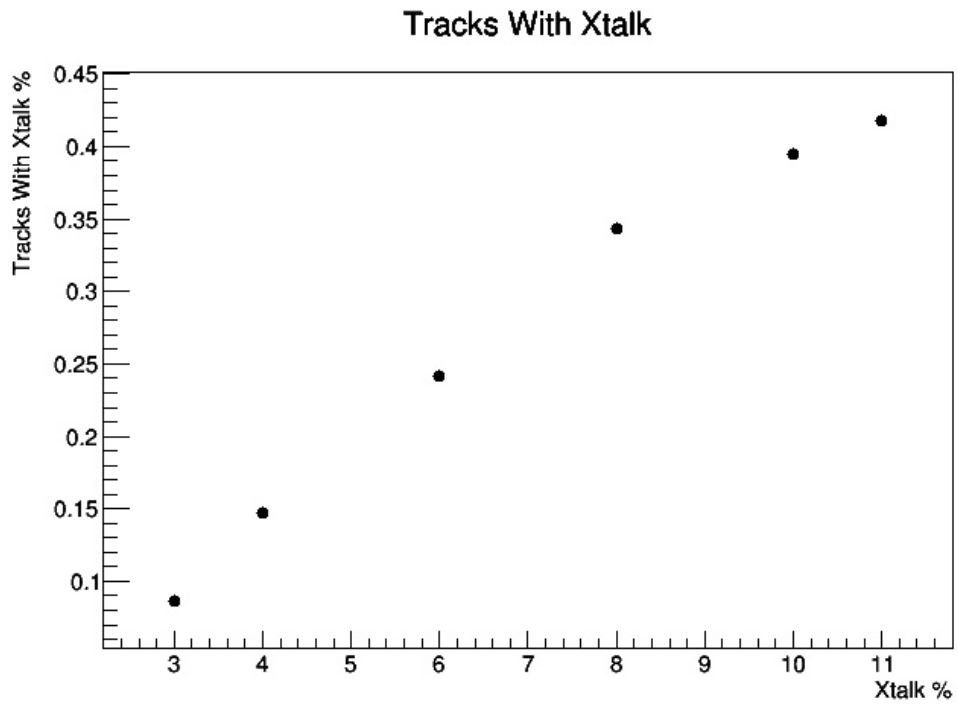

Figure 4.15: Number of tracks with cross talk that are found anywhere in them

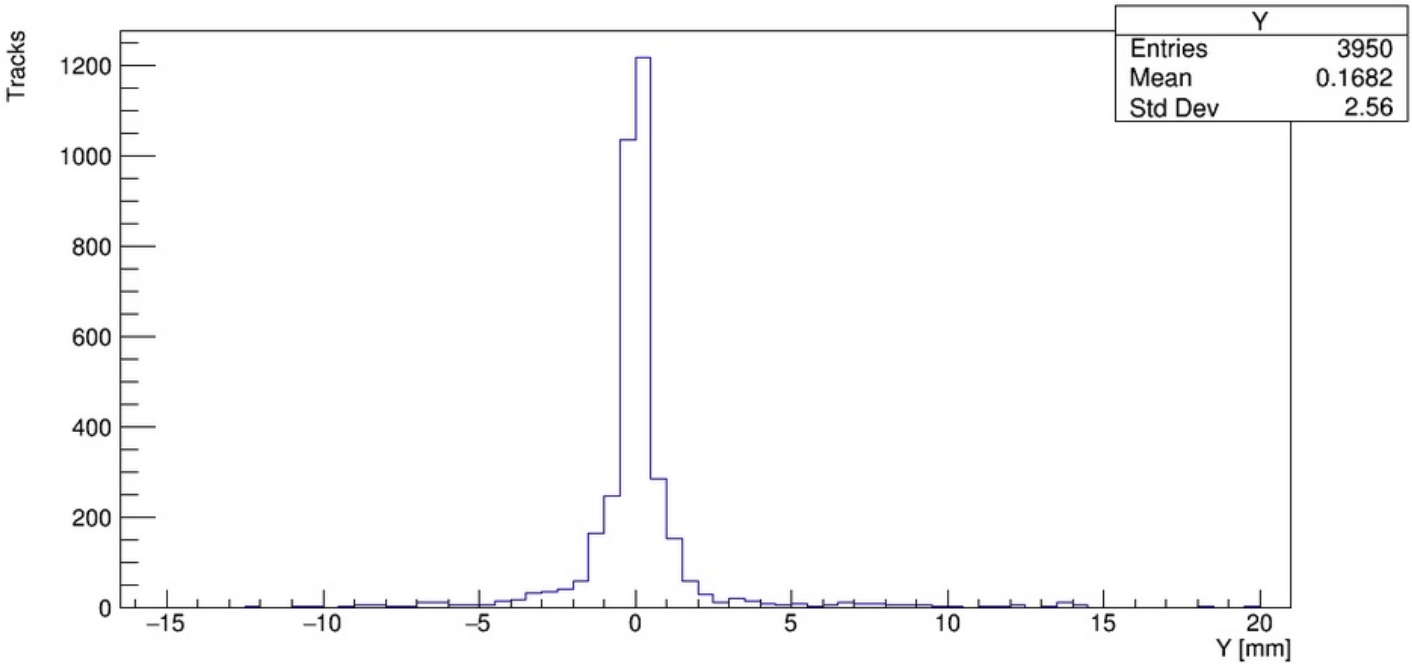

Figure 4.16: The Difference in Vertical positions in tracks with Cross Talk

of that hit. This is an important parameter since this establishes how well we are able to fit the track in the end. The resolution can change throughout the course of data collection and therefore the properties of the resolution need to be established and the effect of the changes of the resolution need to be properly evaluated.

4.2.1 General Explanation of Hit Resolution

The hit resolution in the straw trackers is determined from our ability to model the distance of closest approach to the corresponding drift times. The resolution is defined by the model of the radius to time determination of the straws, which is our modeled drift time vs the distance of closest approach. This model can change with different gasses, pressures temperatures of the surrounding environment. In addition, our model can change with variances in the voltage applied to the detectors.

4.2.2 Evaluation of Changes in Hit Resolution

To evaluate of time to radius distribution it is needed to find a way to observe and model the time to radius distribution in the straw tracker. To do this there was a method developed by James Mott [24] which was called the missing layers experiment. In the missing layers experiment there were a particular selection of tracks, and then there was removed a particular layer from the tracking algorithm so that we can look at where the fitted track lands on a wire without having the fitting process effect the results. This would be the actual distance of closest approach, and then there was observed the corresponding drift times. Please refer to Fig. 4.17 which gives a pictorial representation of the experiment.

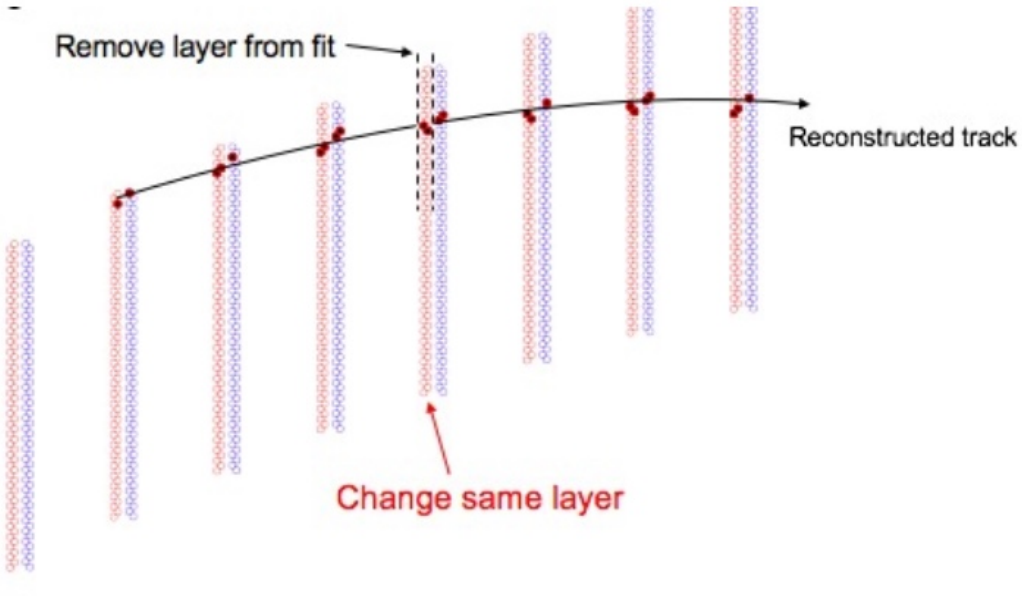

Figure 4.17: A pictorial representation of the missing layers experiment

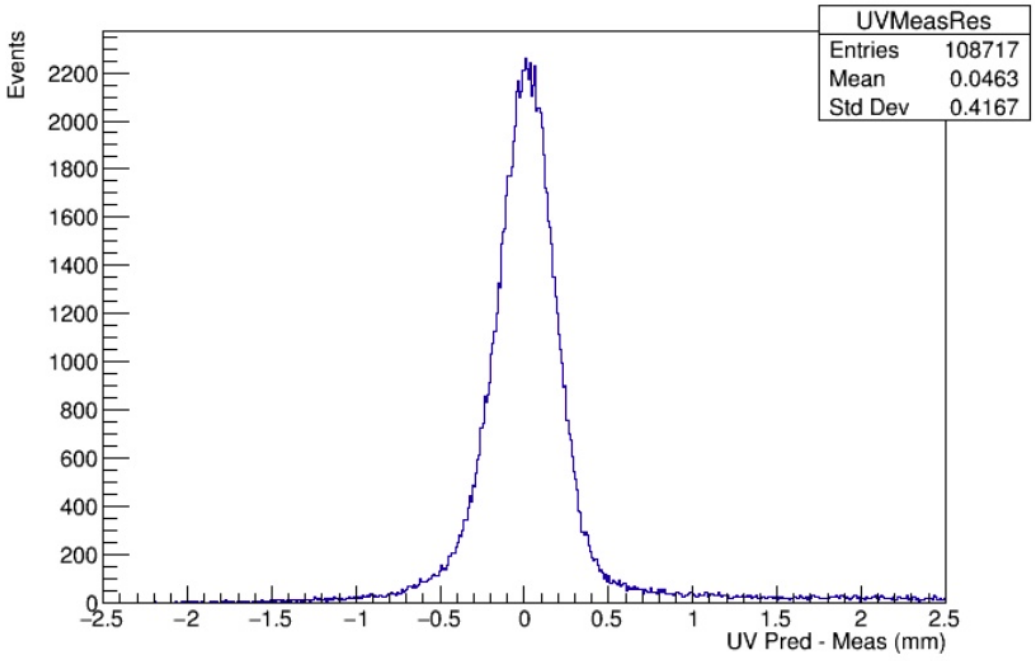

Figure 4.18: Resolution with no track cuts

If we look at this data with no particular tracks selections , found in Fig. 4.18 , we can see that there are tails associated with this semi-gaussian distribution. These tails make it difficult to fit the distribution and also skews our results for our characterization and it was necessary to look at these tracks that fall on the edge of the distribution as to improve our characterization and results. To do so we looked at a small subsection of these tracks with a plotting program that showed these tracks so that we could see what was going on. It was found that there were multiple different cases were the tracks were not properly representing the data that we wanted to look at. Firstly, corresponding to the previous section we have some cases were there might be cross talk or other similar effects, so here we required that is one digit per layer for each track so that we are not looking at the variances of cross talk. Secondly, to simplify the situation and to minimize the chance of error since there may be a lot of other things going on in the code, we required that for a particular time island that there is only one track going through the detectors at a time. By looking at the tracks we found a couple particular cases that happed pretty often. One case it was found that a good portion of the tracks in the outliers were tracks that ended or began on the particular layer that we are studying. Here the track fitting with this missing layer caused the track fitting to not properly represent the true trajectory of the tracks and skewing our results. This was fixed by requiring that the tracks does not begin a couple of layers before and cannot end a couple of layers after the track. The next case that we found was tracks that there were extremely short tracks and they only hit a couple of layers. This causes the track fitting to be less precise due just to the shear number of data points given in the track. To evaluate how many digits that we needed the tracks to get rid of the tracks that are not being properly represented, we looked at the standard deviations of the resolution vs. the number of digits in the tracks found in Fig.4.19, Here you notice that we start to get a the large tails at when there is about 12 digits in the tracks, therefore we required that there are more than 12 digits in the track for this particular study. Another common case of the outliers that

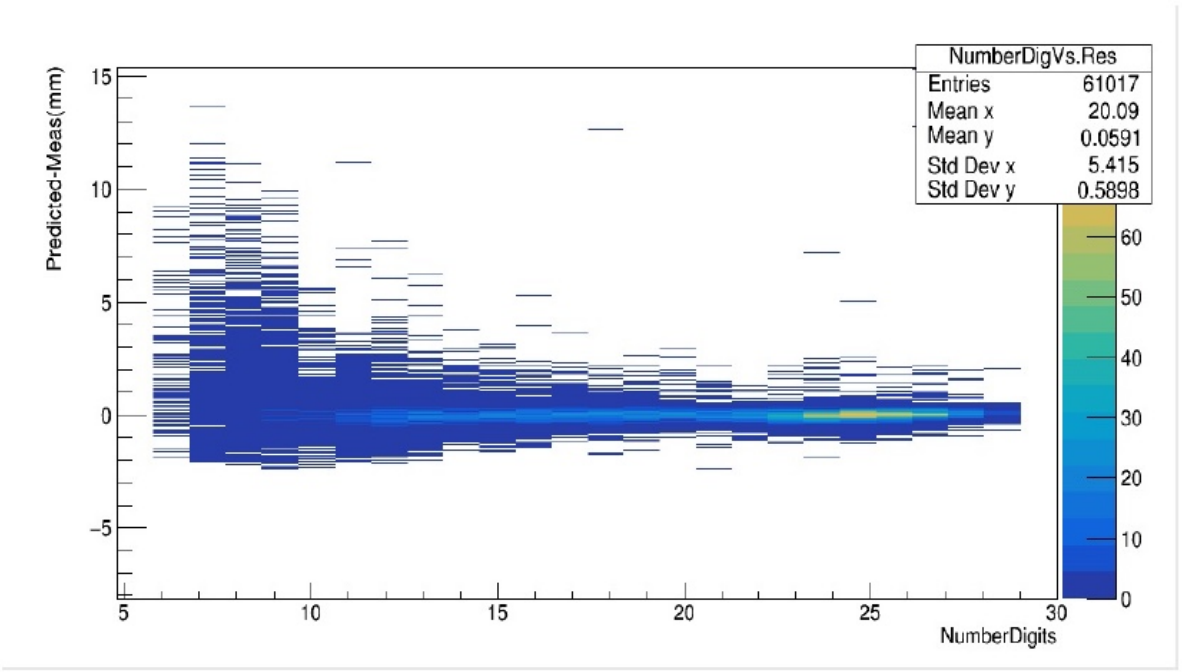

Figure 4.19: The Number of digits associated with a track vs. the Resolution

we found was the case where the particle in the track reflected off of something at the layer that we were trying to study as found in Fig. 4.20. Here this is a problem because before we removed the layer this track would normally fail, however when we removed that layer this causes the chi squared value does not deviate out of range causing the tracks to not fail. To take care of the majority of these tracks we just put a more stringent cut on where the track begins and ends further improving our results.

To show the effects of the previously established track selection I looked at what is called the distance of closest approach efficiency at the layer that was being studied. This will tell us how effectively we were able to predict the distance of closest approach which would show us if we had an improper track selection. To make this plot, first there was made a histogram of all the predicted distance of closest approach, as found in Fig. 4.21, and there was made a histogram of the predicted track position minus the position of the wires in the

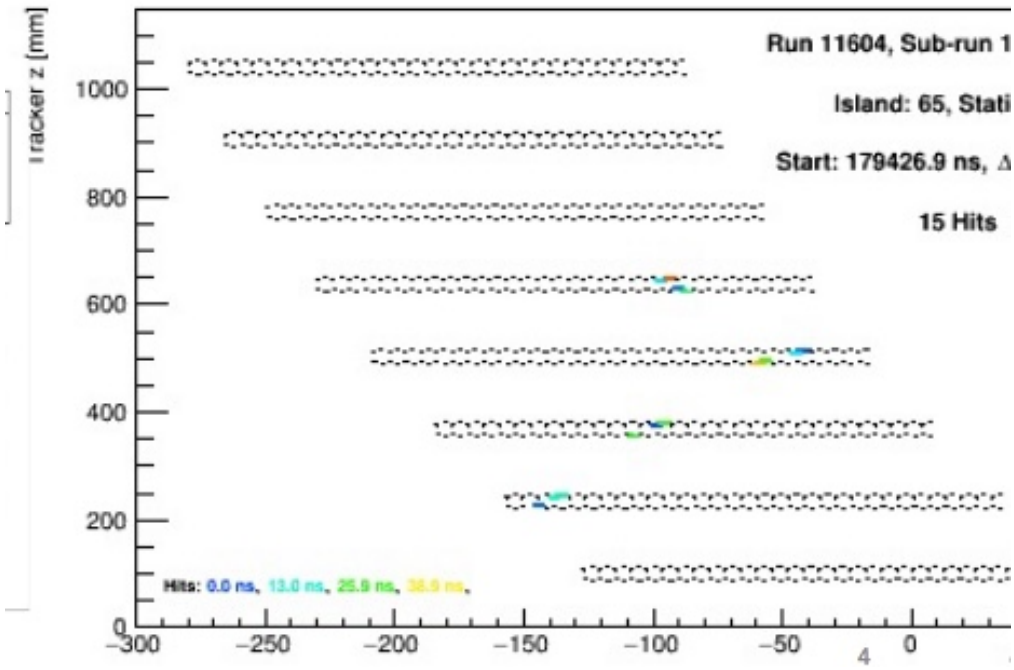

Figure 4.20: An example of a track being reflected off a boundary

layer, as found in Fig. 4.22. With the predicted distance of closest approach histogram is then divided by tracks positions histogram and normalized to the number of wires found in that layer. This will give what we call the distance of closest approach efficiency as found in Fig. fig:badDCAeff. This previous figure gives us our initial results before the tracks selection which establishes that if the tracks hits a particular straw in the layer, which is less than 3mm, it is seen that we are only predicting 90% of our tracks. This result is definitely not correct since if a particle hits a straw we should be able to detect this. Now, If we look at Fig. 4.24 with our current tracks selection we can see similarly that we have a 99% efficiency which is a more reasonable number and tells us that we are more effectively measuring the resolution. Now if we look at the resolution distribution before which is found in Fig. 4.18 and the resolutions distribution after, Fig. 4.26, with most of the tails of this distribution

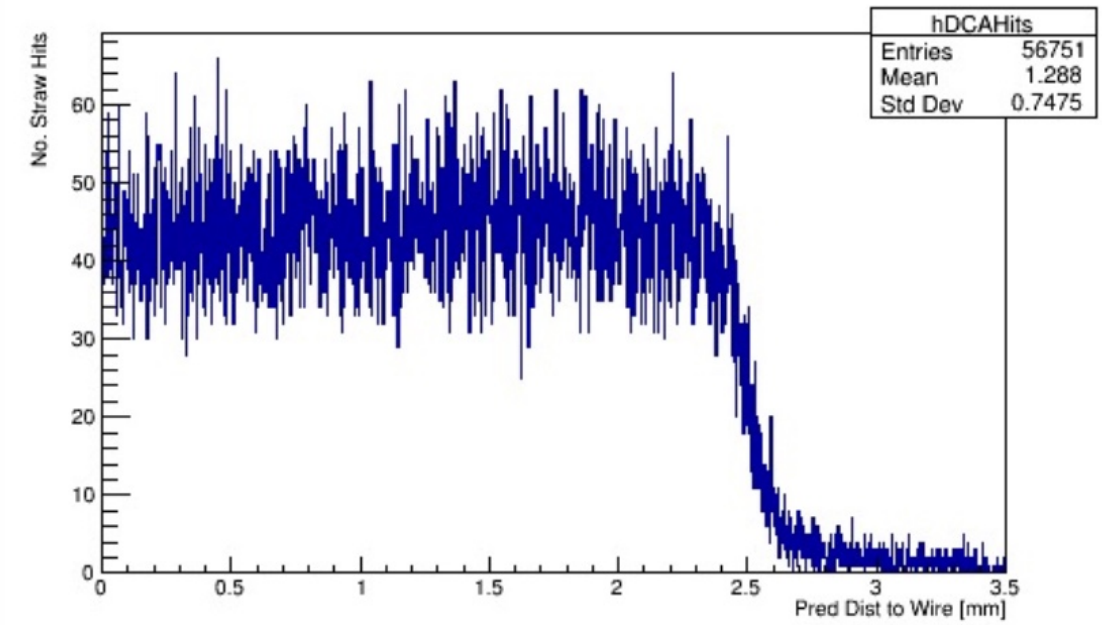

Figure 4.21: All the predicted DCA Hits

are now pretty much gone and the distribution looks more gaussian with a smaller standard deviation.

Another thing to effectively measure the property of the resolution we needed to fit this function with an appropriate function. Although, this function looks fairly gaussian, which is what should happen when measuring the resolution, if we fit to a gaussian we can see we are not effectively fitting this histogram, found in Fig. 4.25. This deviation in the histogram from being a true gaussian occurs because what is actually being measured is a couple of different resolutions occurring at the same time, we have the resolution of our track fitting algorithm and we have the resolution of our distance of closest approach model. In addition, we have the effects of the gas that we are using along with timing differences in the detectors...etc. Knowing this there is a motivation to fit this function to multiple gaussians, one fixed at the core and another one to broadly overly to take in account the tails in the distribution. In

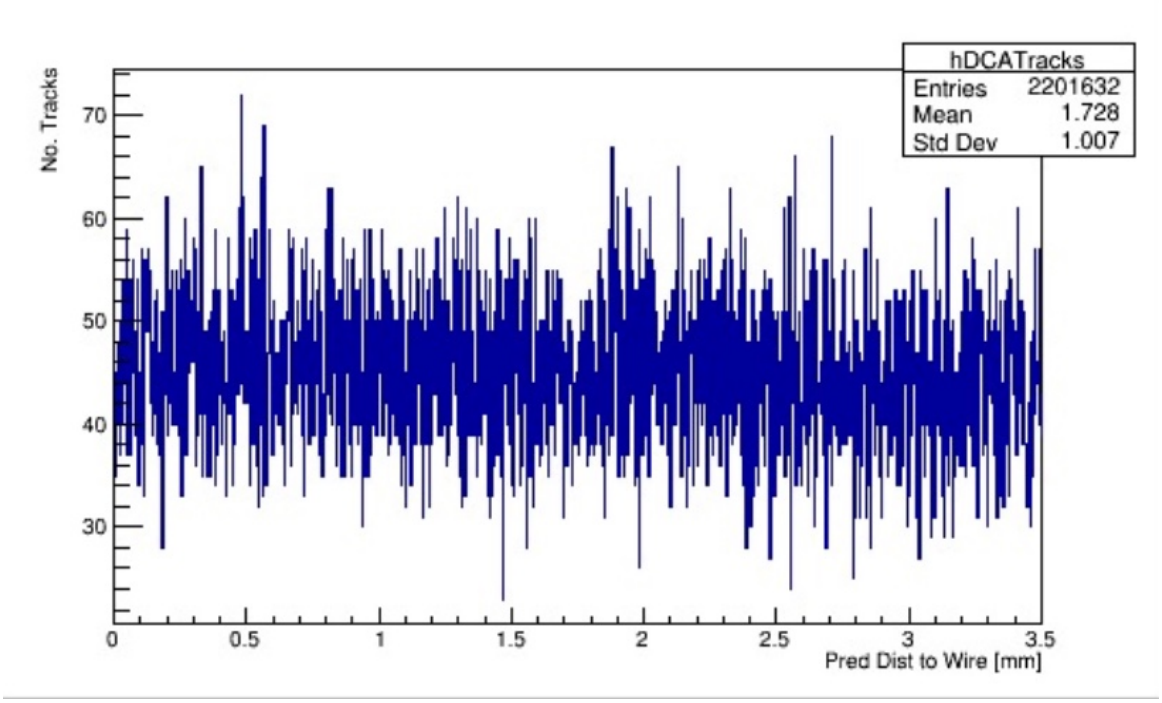

Figure 4.22: All the DCA's determined by the track postion

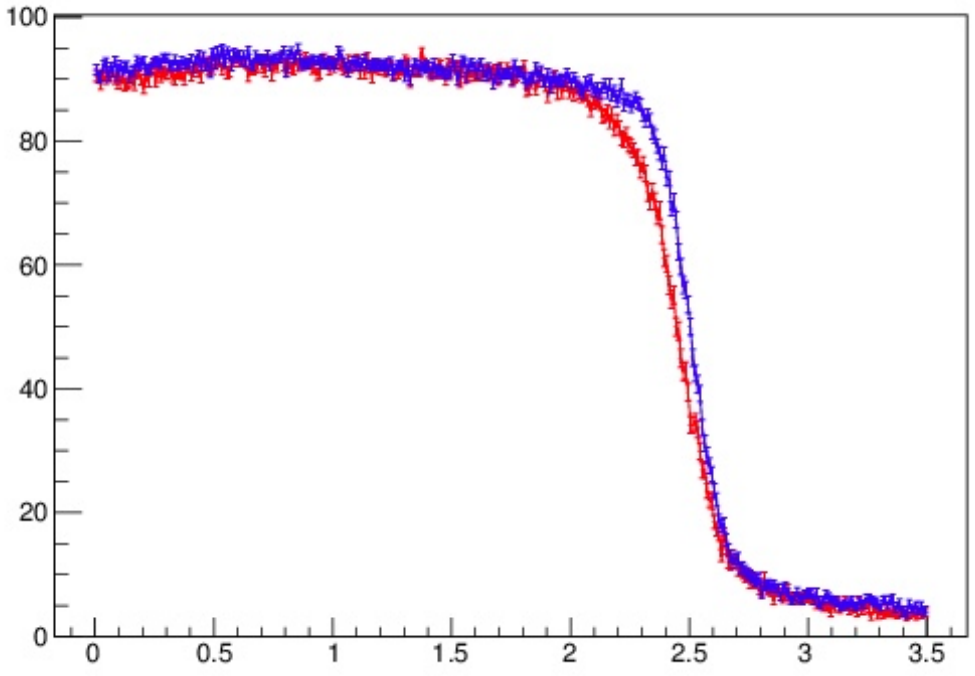

Figure 4.23: The DCA Efficiency with poor track selection black is 1550V red is1660V

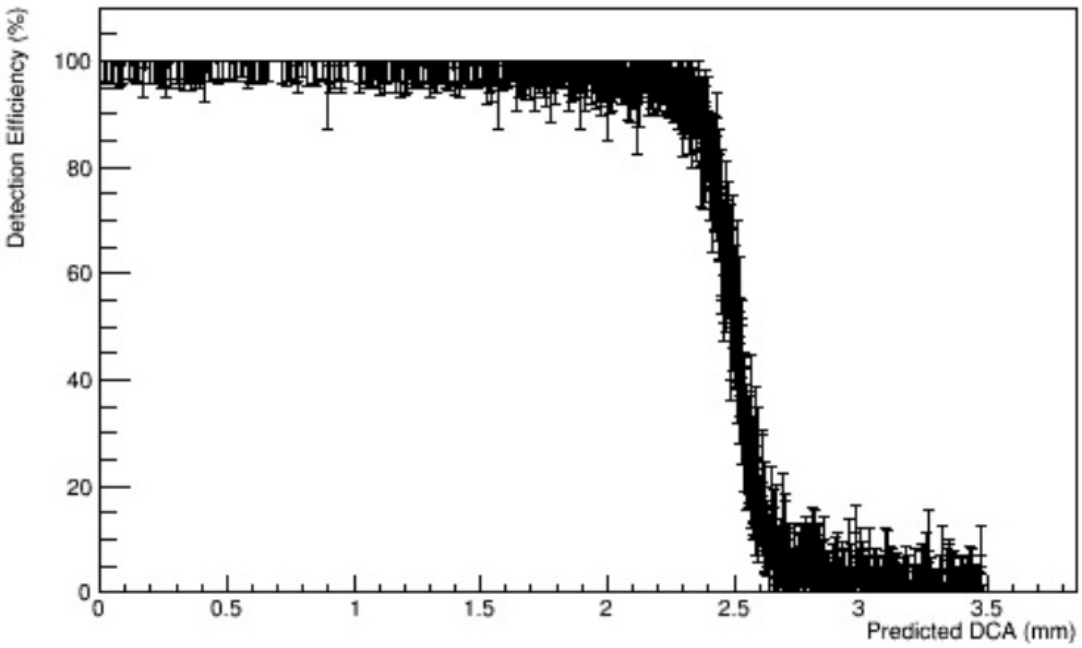

Figure 4.24: The DCA Effienciency

Fig.4.26 is an example of the new fitting method which shows that we get a well established fitting function for the resolution plot. Then the overall distribution standard deviation by adding the standard deviations based on there mean in quadrature. Now that it is established the method to evaluate the resolution we now what causes deviations in the hit resolution.

4.2.3 Evaluation of Changes of Resolution

Using the methods establish in the previous section we now want to talk a look at how the resolution varies for changes in voltages, temperatures, pressures, and from run to run. This is important to understand how to model the changes in a simulation as to study how much of an effect this has on our data, and gives us information on how we can further improve the resolution of the detectors.

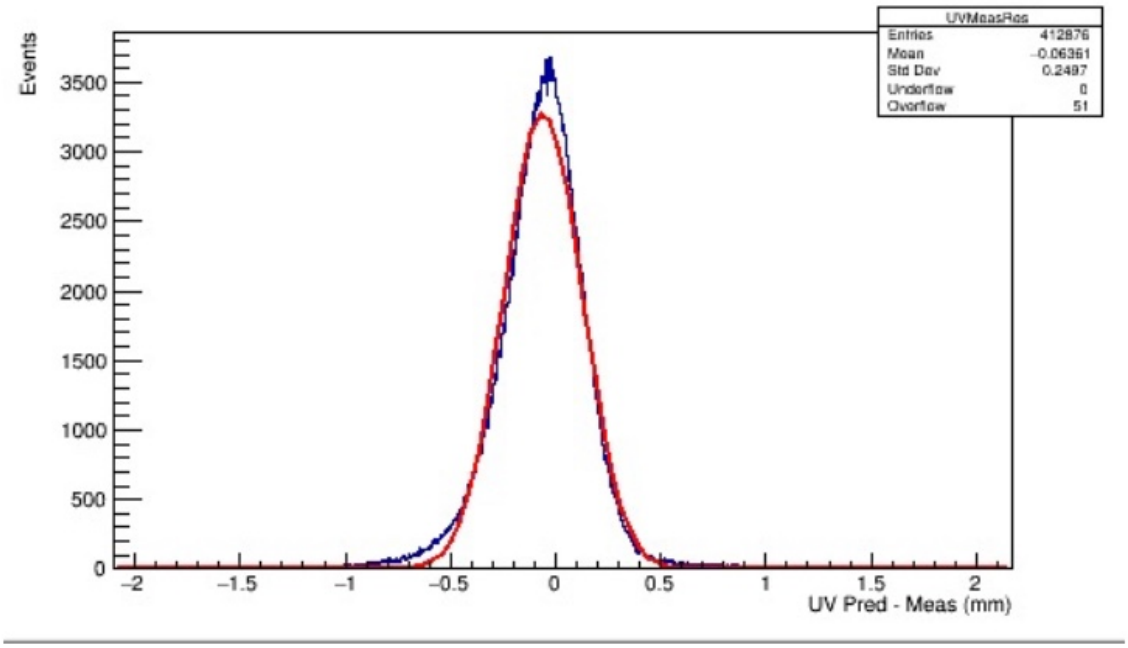

Figure 4.25: Resolution with poor fitting

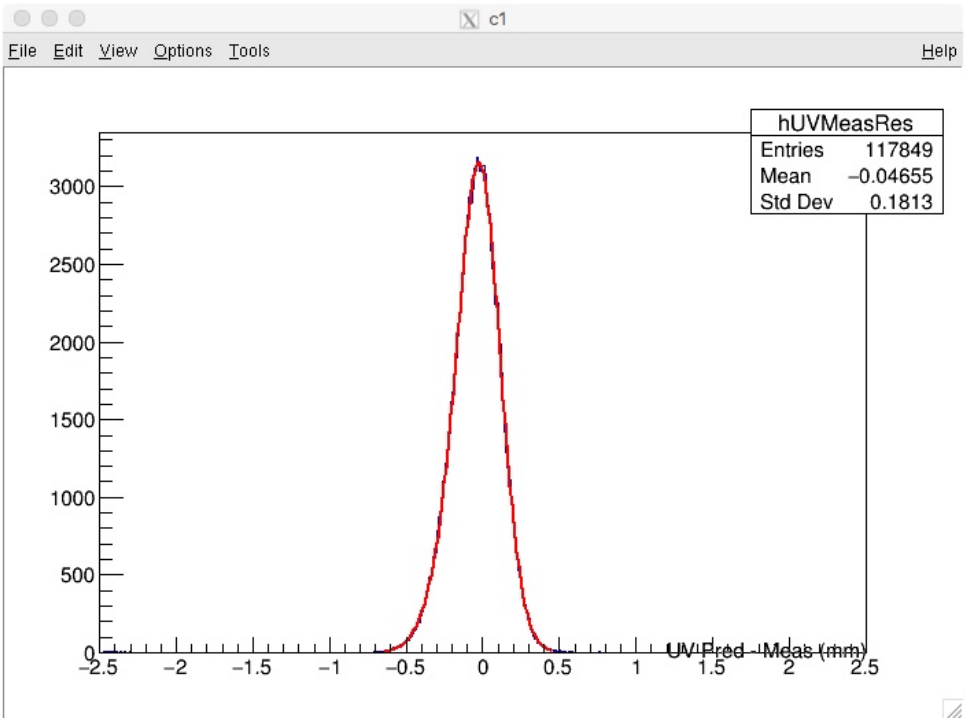

Figure 4.26: Resolution with the proper track cuts and good fit

The first study that was done was called the HV Scans experiment. Here when the beam was on there were tracks collected when we varied the voltage on the detector for the particular layers that we were studying, while keeping all the other detectors the same. Now this tells us how our model deviates vs.changes in voltages without ever affecting the track fitting process which gives us the effect that we are looking for. Here we studied both stations (12, 18) and looked at the 3rd tracker in the first two layers from the direction of the beam which gives us a good example of tracks in the middle of the detector. In Fig.4.27 it is seen that we definitely get a variance due to voltage changes which is expected however, we can see from the plot that we only get a variance of 0.04mm over the course of 160 Volts. This is a large voltage variation as compared to the variation that we would expect under normal conditions. Notice, that we get better resolution as we increase the voltage, this is due to the fact that as we get higher voltages we get larger deviations in the drift times and we are more able to pick out the distance of closest approach according to the model. In addition, notice that we also get fairly large deviations in the plot away from the linear relationship that this seems to follow, this follows from the fact that this data was collected over a period of 12 hours and there could be large deviations in all the other parameters that could effect the resolution, therefore these deviations are not out of line.

For the rest of the studies of the resolution it is necessary to have significant amount of data collected over a large period of time, here the what is called the 60 hour data set was used. As it sounds this was data that was collected with over a continuous 60 hour period. In Fig 4.28 there is the resolution for layers 44, 45, 76 ,and 77 from run to run we can observe that there is roughly a 10% deviation in the resolution over the course of the experiment. Here the error bars are given by the fitting errors established in the previous section. Furthermore, to investigate how much the resolution varies over the course of the run I took two runs and measured the resolution in subset of 10 sub-runs and looked at the

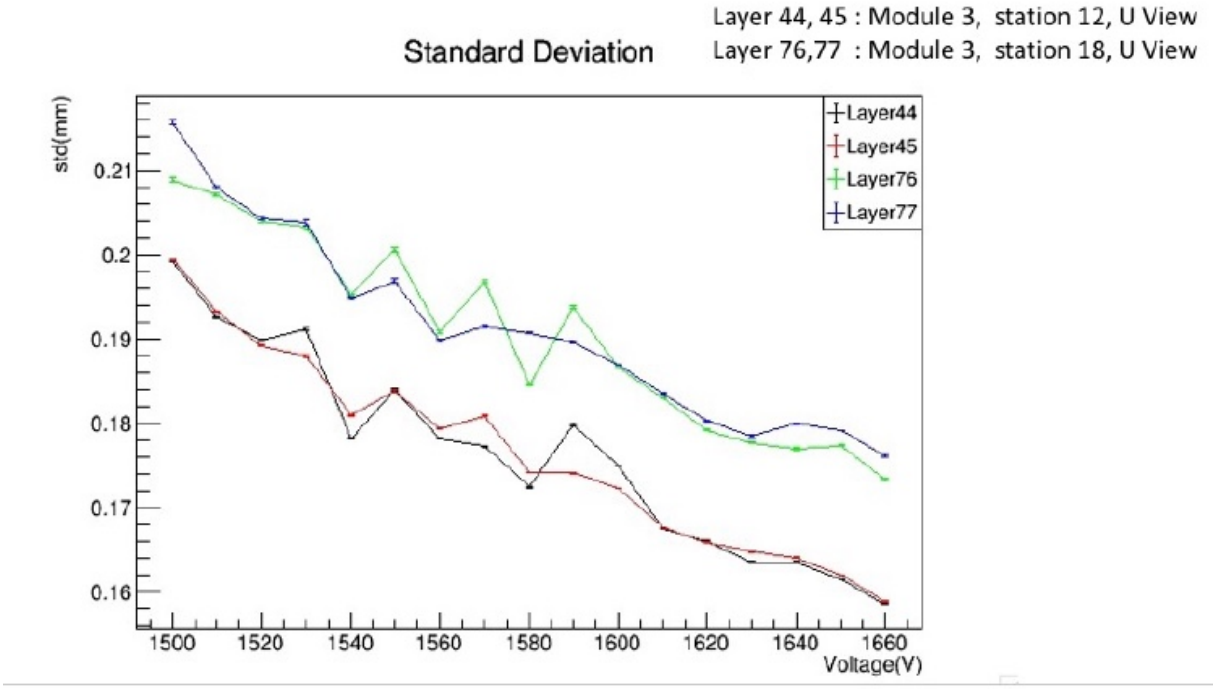

Figure 4.27: Resolution vs Voltage

resolution, this is found in Fig.4.36 which shows that there is approximately 13% variance over the course of the run.

Now that we have this data we can look at the average pressures, temperatures, and humidity over the course of these runs. In Fig. **??** is how the temperature in the experiment room varies over the course of data collection which we can see there is quite a large variance. Next, by looking at the average temperature over the course of a run vs. the resolutions from run by run , Fig. **??**, we can see that there is no significant correlation between temperature and resolution changes with a Pearson correlation coefficient of 0.0643078. It was shown by another scholar that the track fitting changed with temperature by plotting the chi squared value vs. the temperature as shown in Fig. **??** which was expected to be from the resolution changes but it was shown that was not the case. To make sure this is the case it was investigated for my track selection that the chi squared values vs. temperature

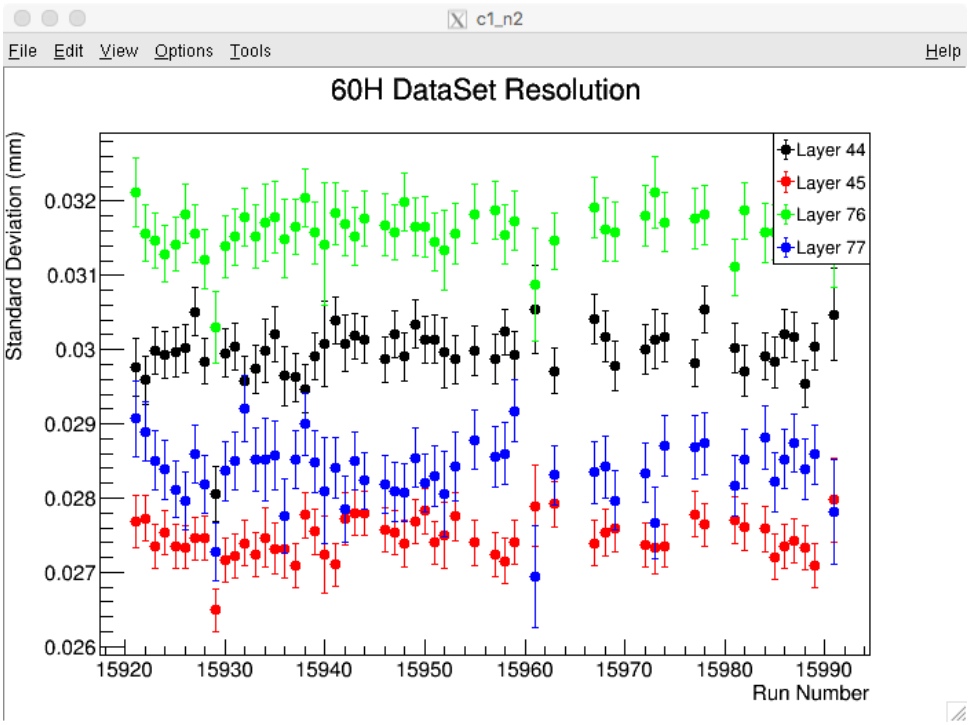

Figure 4.28: Resolution Vs. Run Number

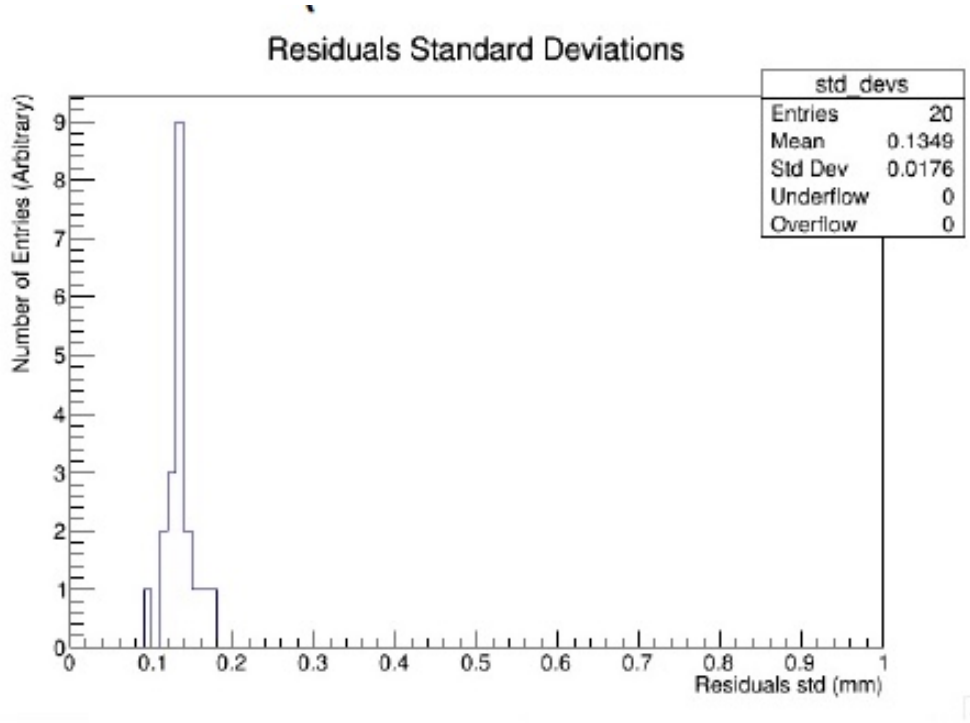

Figure 4.29: Resolution Over Two Runs

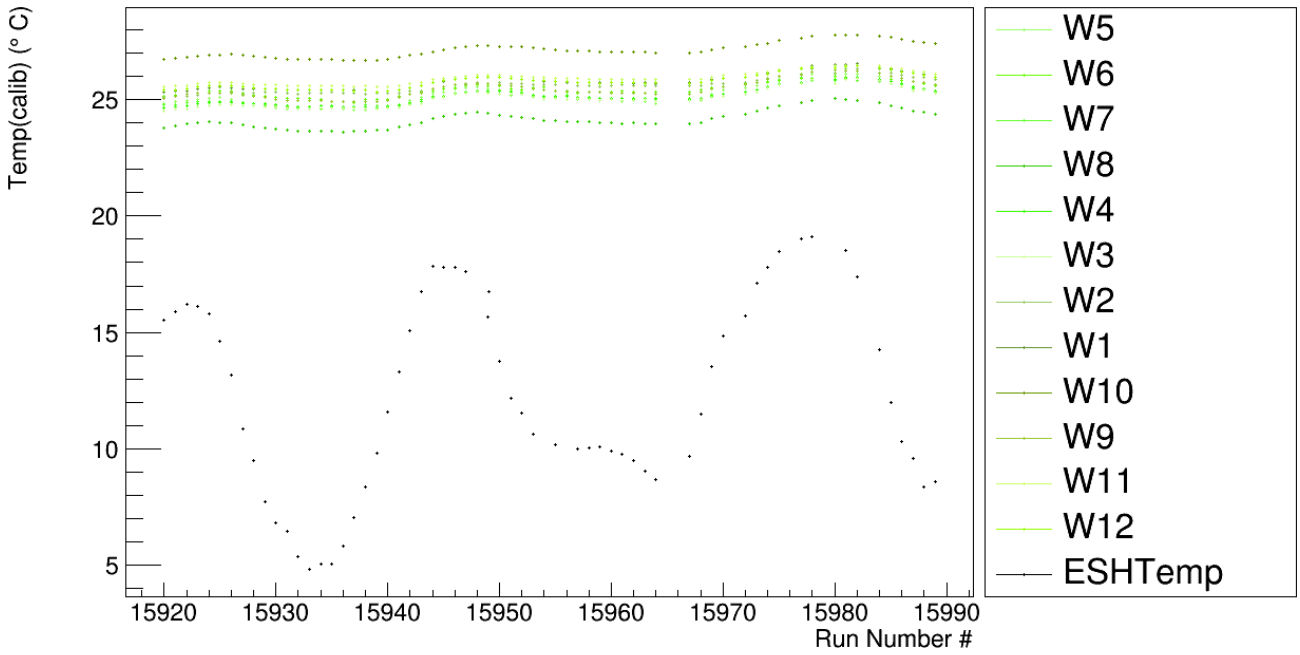

Figure 4.30: Temperature Vs Run Number

didn't change. Shown in Fig. 4.33 and Fig. 4.34 shows the mean and standard deviations of the chi squared values do not vary with the temperature and have a small correlation factor. Therefore this reaffirmed by previous statement in saying the resolution was not significantly dependent on temperature in addition to saying that the deviation in the chi squared values vs. temperature was caused by something else that would bias the tracks.

Next the correlation between pressures and resolutions were investigated in a similar way to the temperatures. In Fig. **??**show how the pressure varied over the course of the runs that we are investigating. This shows that there is a changes of in pressure over the course of the collected data and this variation would show us if there were any changes of the resolution over normal pressure variances that we would see over the course of the experiment. Looking at the average pressure vs. resolution averaged from run to run, **??**, again shows that there is no significant correlation between pressure and the resolution with

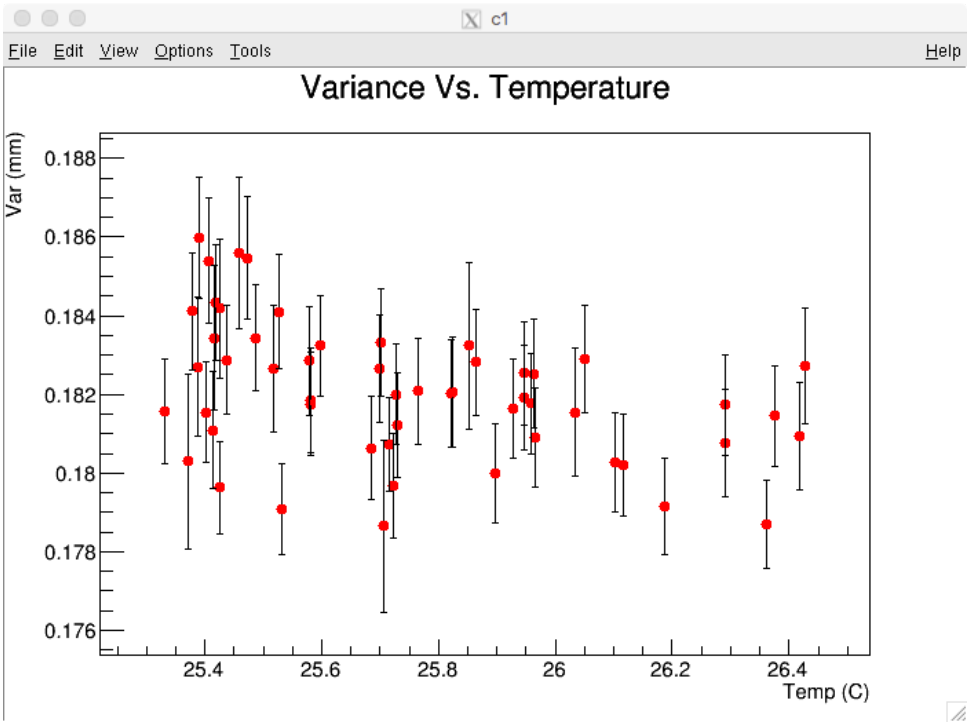

Figure 4.31: Resolution Vs. Temperature

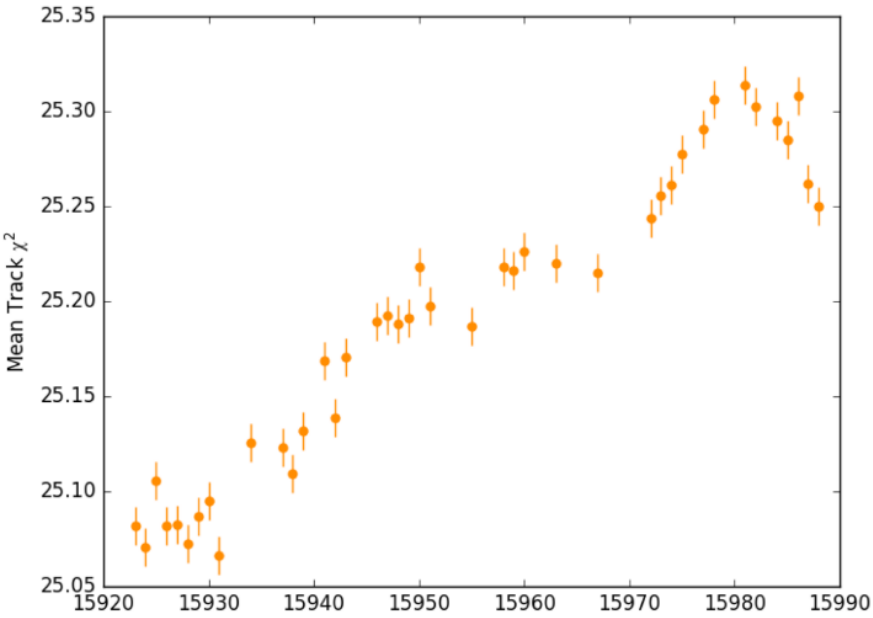

Figure 4.32: Mean Chi2 over 60H Data Set

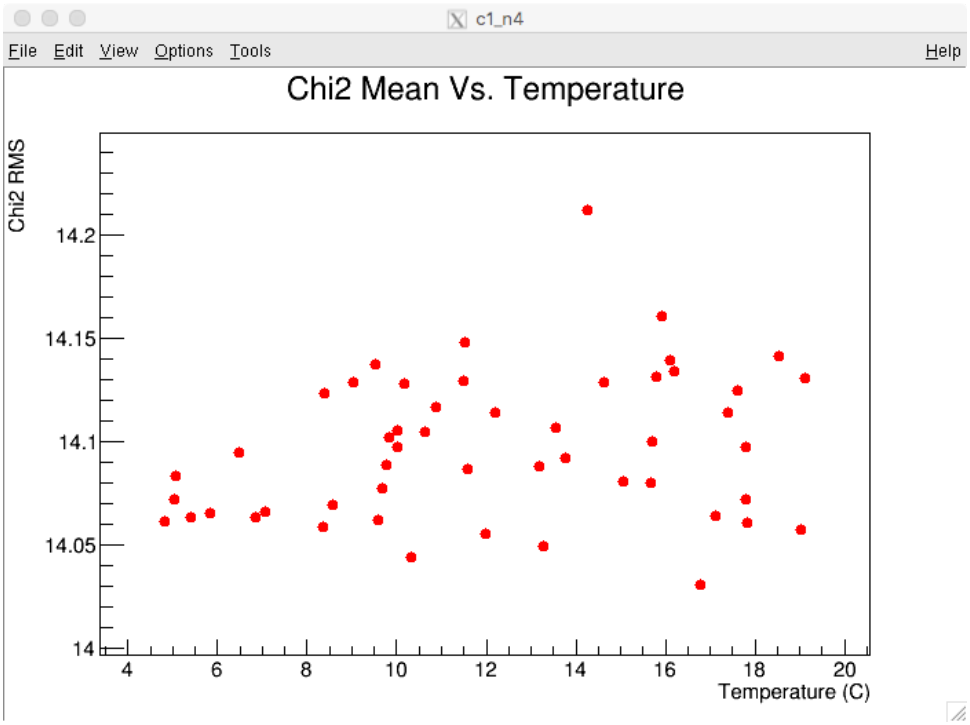

Figure 4.33: Chi2 Mean Vs. Temperature

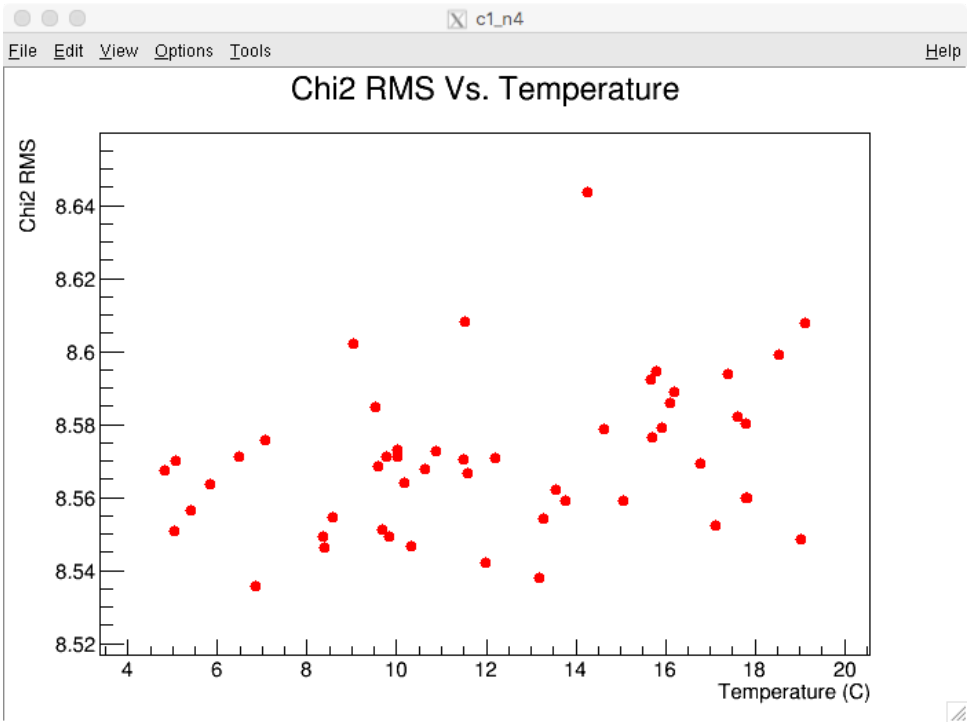

Figure 4.34: Chi2 RMS Vs. Temperature

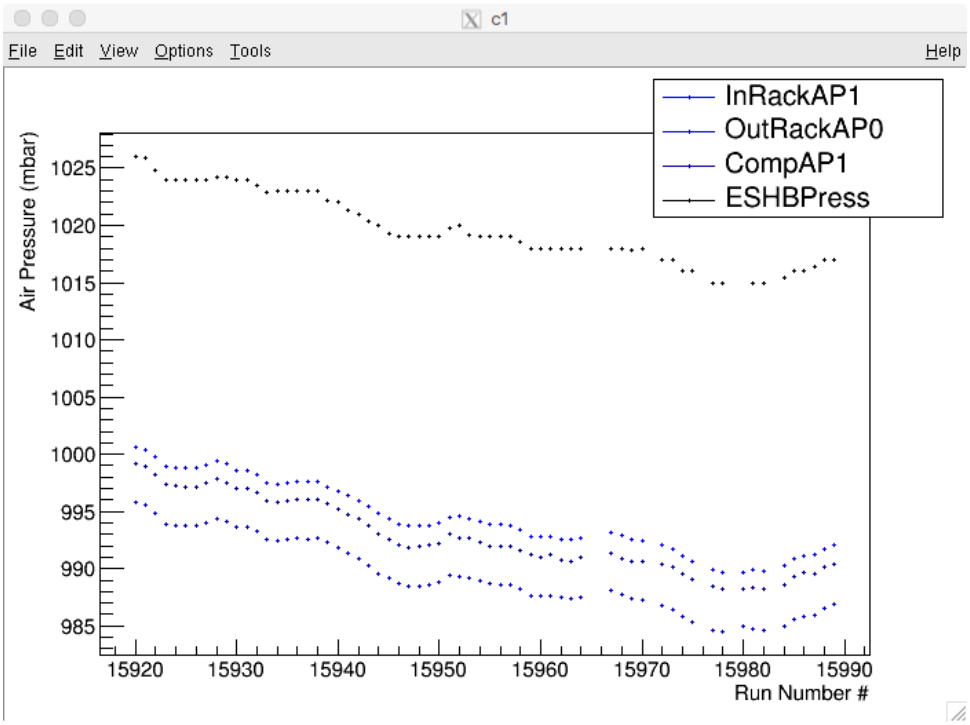

Figure 4.35: Pressure Vs. Temperature

no significant correlation factor. Similarly, it was shown that the chi squared values varied vs. pressure again we wanted to make sure that this was not due to the resolution. Shown in Fig. reffig:chiMeanPresand Fig. 4.38shows the mean and standard deviations of the chi squared values do not vary and the variance is caused by some other changes in the tracks vs. pressure.

Now we have shown that for the effects that were established there is no significant effects on the resolution of the trackers. We also observed the amount that we would expect the tracker resolution to change over the course of the experiment which allows us to investigate how much of an effect this has on our final results.

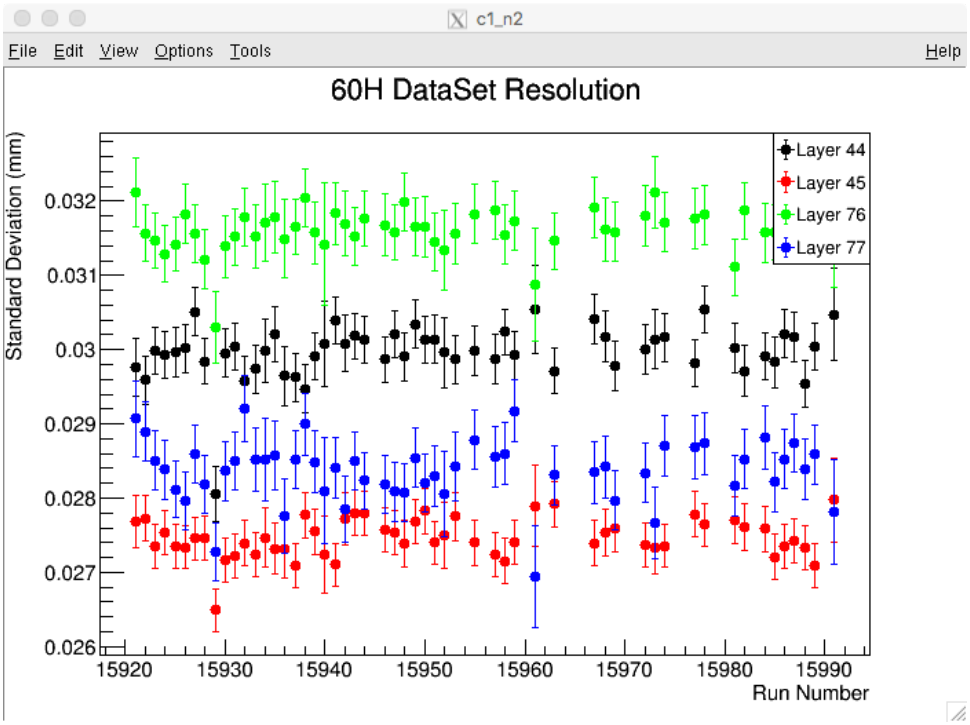

Figure 4.36: Resolution Vs. RunNumber

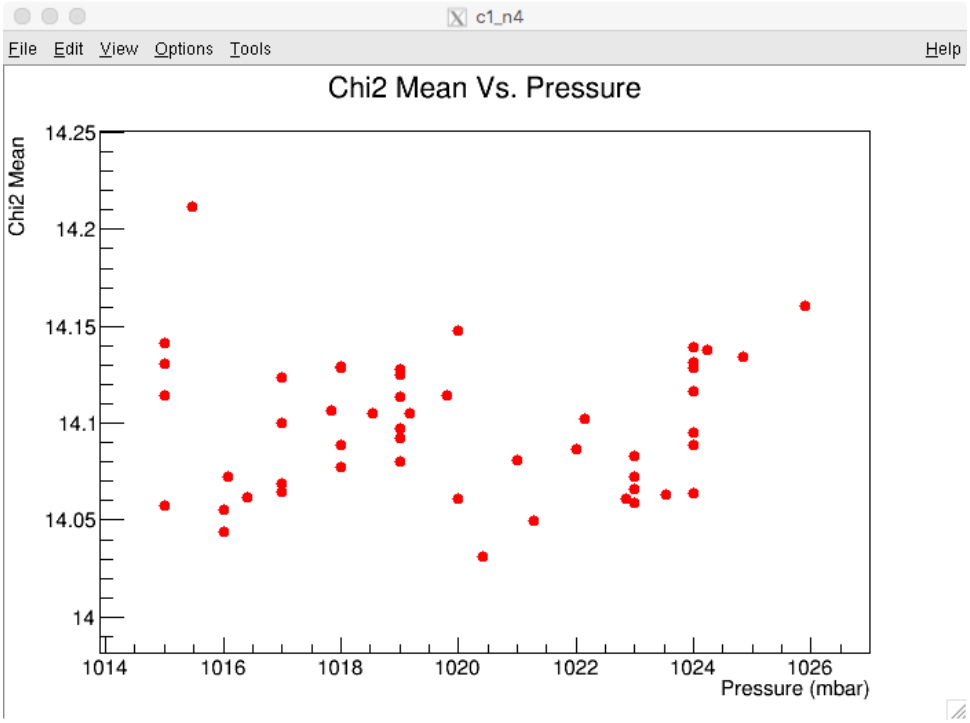

Figure 4.37: Chi2 Mean Vs. Pressure

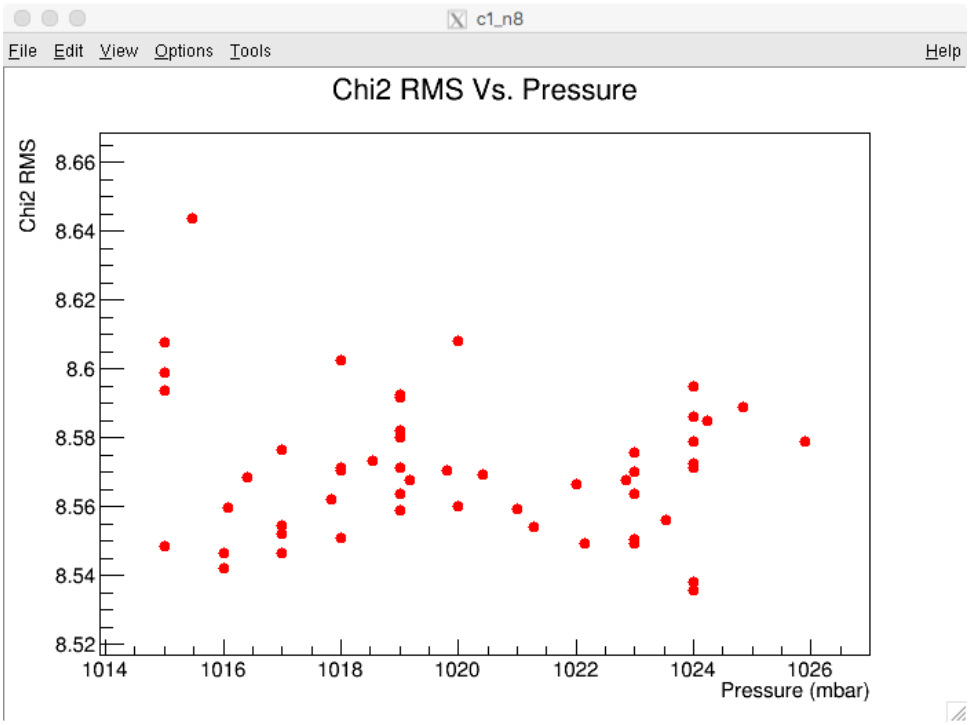

Figure 4.38: Chi2 RMS Vs. Pressure

4.2.4 Changing Hit Resolution in Data

Now that we establish what causes changes and how much each effect causes changes in the hit resolution it is necessary to evaluate how much the changes affect our final results. To do so we took a look at one particular data set that has a given resolution value (This data was taken from one of the runs of the 60 hour data set) and randomly varied according to a gaussian distribution the distance of closest approach to some standard deviation value. This will give us the same effect as the resolution varying and we can look at how the extrapolation changes the vertical and radial distributions which is our main contribution to errors, as previously established. Practically, to do this experiment there was directly added in a section of code that randomly selects a value according to a gaussian distribution with a defined standard deviation and mean of zero. Then this randomly generated value was

added to the distance of closest approach and passed this on to the rest of the code in the tracking algorithm.

Next we needed to see how much the radial and vertical position distributions are effected. In the previous section we showed that over the course of a run that there is a 13% variance in resolution. Looking at the extrapolated y positions vs. different smearing percentages, Fig. **??** , you can find that the average y position at 13% only varies by a small amoun (Here the red line is at 13%) . Even if we vary the resolution by 100% the average y position changes by 3mm which is small compared to the other error contributions covered. Similarly, if we look at the standard deviation of the extrapolated vertical position vs smearing Fig. 4.41, we only see changes of 0.05mm at 13% and 5mm at 100% which also shows that this number is also not severely affected by the resolution changes by the numbers we have. Looking at the same plots except for the radial distribution we only, Fig. 4.42 and Fig. 4.43, we only observe 0.05mm of a change in the average radial position and 0.2mm change in radial standard deviation at the 13% mark which again is a small contribution to the errors.

4.3 Results and Conclusions

In this chapter it has been explained the work that I have done towards trying to understand the systematics and there contributions to the final numbers. In other contributors work It has been found that with the current tracking algorithm that there are many corrections to the tracking algorithms that can be worked towards to improve the results of the EDM analysis. With the work that I have done I have shown that these two main effects that I have studied both the cross talk and the resolution of the detector contribute in a very small fashion. I showed that cross talk will only effect the final numbers to the $<$0.005ppb level in which the largest effects mainly the tracker alignment contribute to the 0.3 ppblevel.

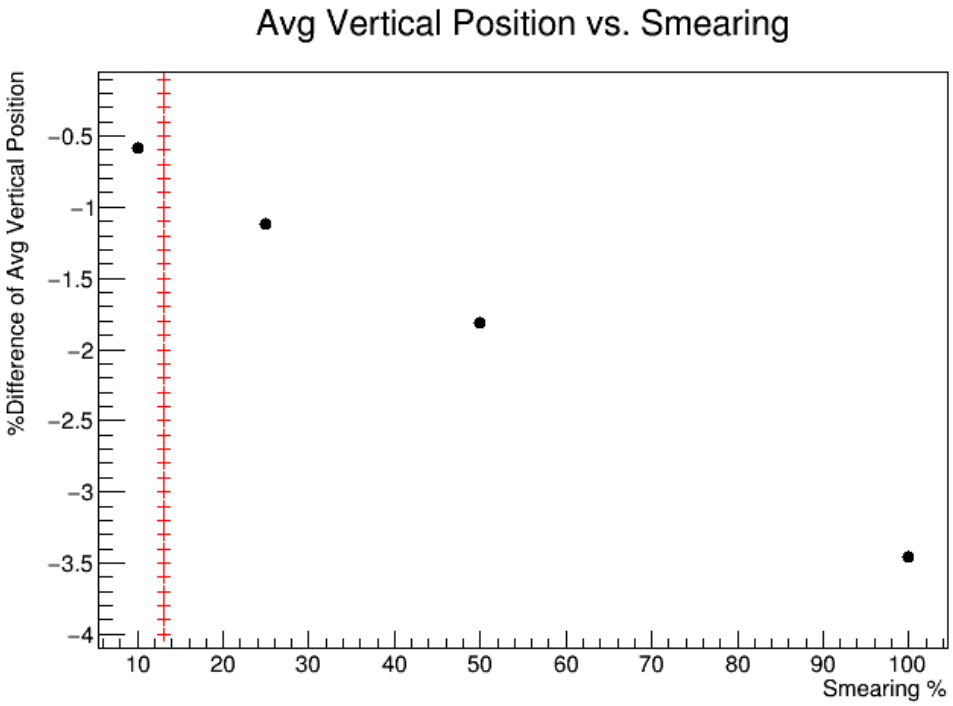

Figure 4.39: Difference in Vertical Position Vs. Smearing

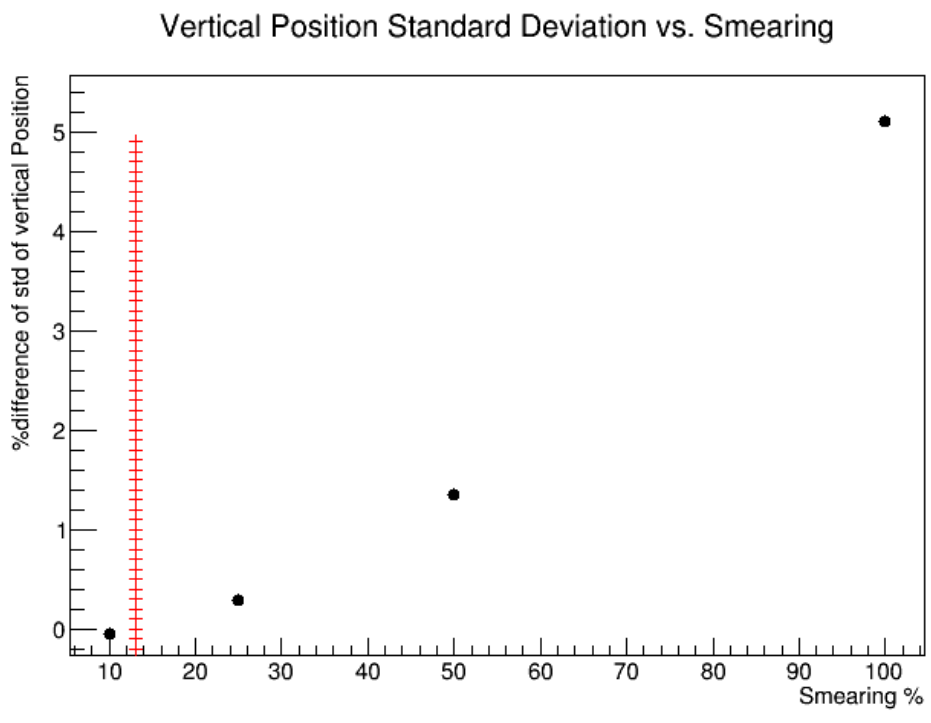

Figure 4.40: Difference in Vertical Position Standard Deviation Vs. Smearing

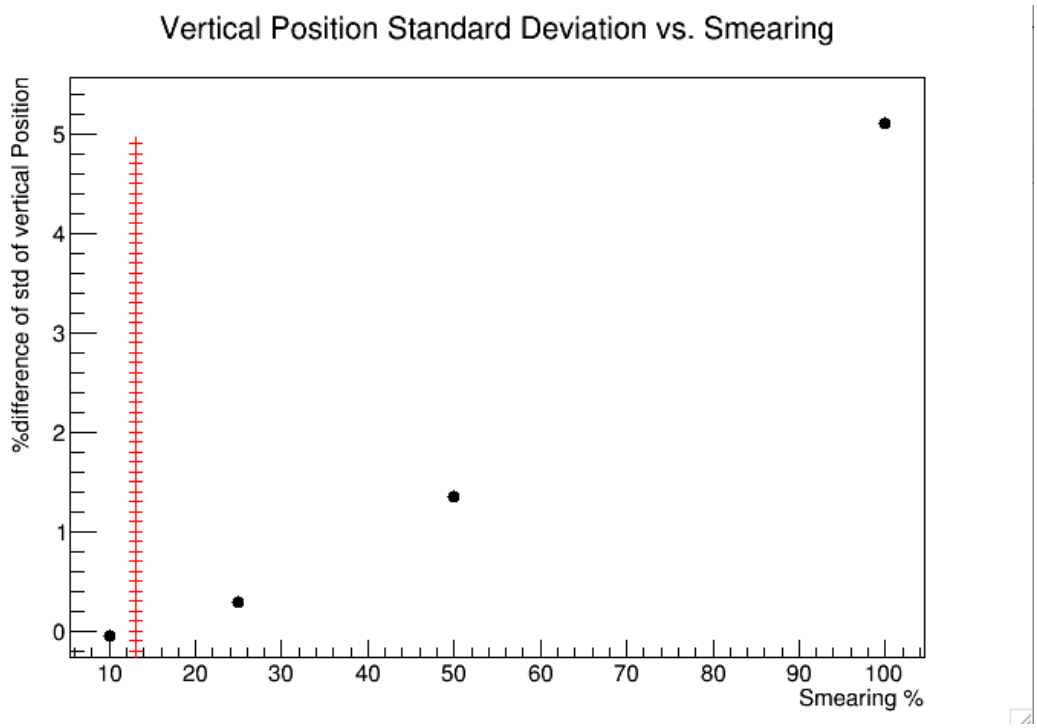

Figure 4.41: Difference in Vertical Position Standard Deviation Vs. Smearing

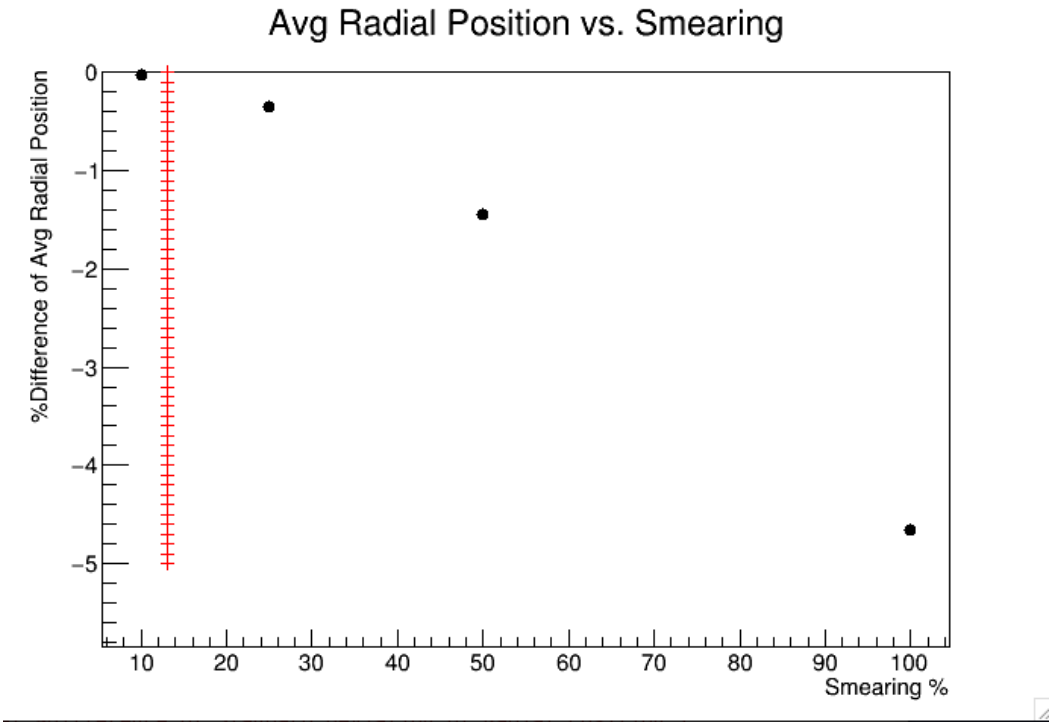

Figure 4.42: Difference in Radial PositionVs. Smearing

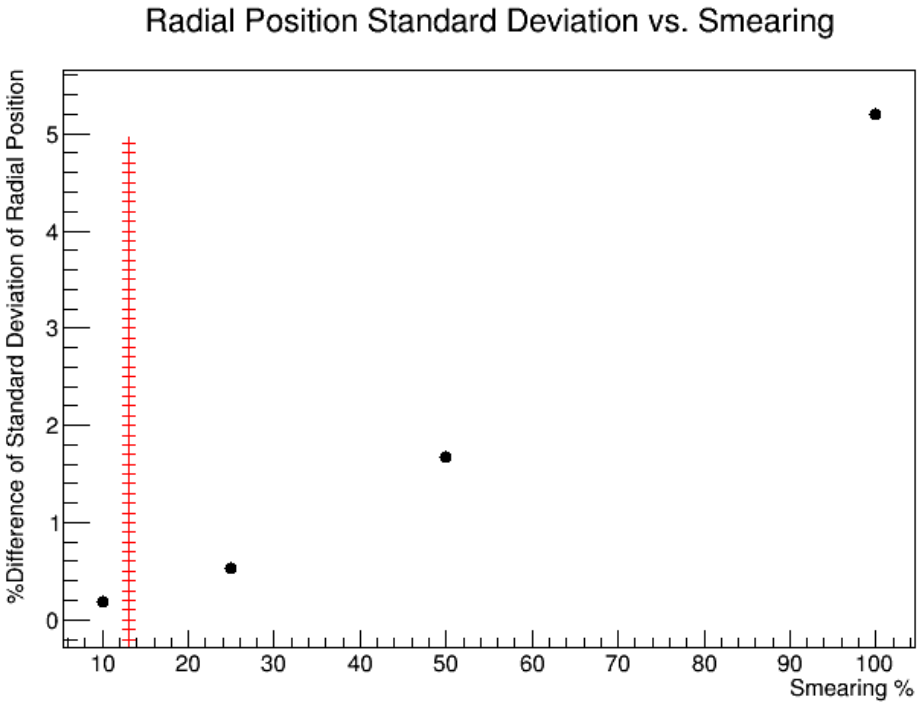

Figure 4.43: Difference in Radial Position Standard Deviation Vs. Smearing

In addition, I have found that due to the resolution changes that we would expect over the course of the experiment and is also small and it effects the final measurement to the 0.03 ppb level. In conclusion, it has been found that there are other areas in the tracking which would contribute more than these errors.

REFERENCES

[1] G. Charpak, F.J.M. Farley, R.L. Garwin, T. Muller, J.C. Sens, and A. Zichichi, Phys. Lett.1, 16 (1962).

[2] J. Bailey et al., Nuovo CimentoA9, 369 (1972).

[3] J. Bailey et al., Nucl. Phys.B150, 1 (1979).

[4] ?? M. E. Crow. Aerodynamic sound emission as a singular perturbation problem. *Stud. Appl. Math.*, 29:21–44, 1968.

[5] W. Gerlach and O. Stern, , Z. Phys.8, 110 (1922); Z. Phys.9and 349(1922), Z. Phys.9, 353 (1924); W. Gerlach and O. Stern, Ann. Phys.74, 673 (1924).

[6] Luis W. Alvarez and F. Bloch, Phys. Rev.57, 111 (1940).

[7] J. Schwinger, Phys. Rev.73(1948) 416, and Phys. Rev.76(1949) 790.

[8] R. Frisch and O. Stern, Z. Phys.85, 4 (1933), and I. Estermann and O. Stern, Z. Phys.85, 17 (1933).

[9] See Figure 5 in Paul Kunze, Z. Phys.83, 1 (1933).

[10] Garwin RL, Hutchinson DP, Penman S, Shapiro G, Phys. Rev. 118:271 (1960)

[11] L. Landau, Nucl. Phys.3, 127 (1957).

[12] A. Epps, Masters Thesis, Northern Illinois University, July 2017

[13] D. Kawall, Fermi National Lab, 49th Annual Users Meeting.

[14] J. Mott, Fermi National Lab , GM2-doc-3195-v1

[15] J. Grange et al. (Muon g-2 Collaboration), arXiv:1501.06858

[16] J.Phys.Conf.Ser. 396 (2012) 022020

[17] J. Price, Fermi National Lab , GM2-doc-4375-v1

[18] Fermi Lab Redmine, https://cdcvs.fnal.gov/redmine/projects/gm2tracker/wiki/Reconstruction_Conte

[19] Fermi Lab Redmine, https://cdcvs.fnal.gov/redmine/projects/gm2tracker/wiki/Digitalization_Conten

[20] J. Mott, Fermi National Lab , GM2-doc-6171-v1

[21] N. Kinnaird, Fermi National Lab , GM2-doc-8102-v3

[22] S. Charity, Masters Thesis, University of Liverpool, September 2018

[23] J. Mott, Fermi National Lab , GM2-doc-17539-v2

[24] Mott. J, Fermi National Lab , GM2-doc-11112-v1